2004年末からは週１回の投与で十分な効果が得られるPegIFNα-2bとリバビリン併用療法が認可された。難治性C型慢性肝炎に対する欧米およびわが国の治験成績での著効率は50%以上を示している。また，週１回の注射でよいことから，副作用も軽度で患者のQOLも良好となり，期待できる治療法である。

C型慢性肝炎に対するIFNの投与は長期間となるため血小板減少，間質性肺炎，うつ病，甲状腺機能異常などの副作用が指摘されており，注意を払う必要がある。

その他の治療として，強力ネオミノファーゲンCおよび小柴胡湯も肝癌発症予防に有効であるとの報告もある。

(5) 一般的な感染予防

B型肝炎の予防の項で述べたように，HCVキャリアへ日常の自己管理と他人への感染予防についてB型肝炎の場合と同様のこと（B型肝炎の項を参照）を指導する必要がある。

性行為によるHCV感染は，セックスパートナーの一方がキャリアである場合に起こる。ワクチンも開発されておらず，コンドームの使用以外，予防方法はないが，幸いに夫婦間感染率も少なく，特別な措置は必要ないと思われる。しかし，特殊浴場女性従業員でのHCV感染率が高いことから[15]，夫婦間以外での性行為による感染の危険は高く，米国のCDCが指導しているように，セックスパートナーを減少させることも，一つの予防対策と考えられる。

(6) HCV暴露後の医療従事者の対応

HCV抗体陰性医療従事者がHCVに暴露した場合，直ちに行うべき対応策はないが，１年間の経過観察を行う。この観察期間にAST/ALTの上昇あるいはHCV抗体が陽性化した場合で，HCVRNAが陽性の場合IFN治療を考慮する。IFN投与は発熱，全身倦怠感などの副作用が強く，その投与には議論もあるが，C型急性肝炎は高率に慢性化するため，慢性化の防止対策としては必須の治療法と考えられる。感染後３ヵ月以内にIFNを投与すれば，４週間の投与期間でも80%が完治し，再発した場合20週間の追加投与を行えばこれらの再発例も完治する[16]。この際のIFN療法はIFN単独投与で十分であり，その効果はgenotype，HCVRNA量とは関連ない。しかし，針刺し事故などでは労働災害として保険適応となっているが，一般の急性肝炎では未だ保険適応ではない。

Ⅱ. 呼吸器ウイルス感染症

■1. インフルエンザ

(1) 特徴

インフルエンザウイルスはオルソミキソウイルス科に属し，さらにA型，B型，C型に分類される。直径80－120nmの球状の粒子で，ヌクレオカプシッド（AおよびB型は８個の遺伝子分節，C型は７個）が脂質二重膜からなるエンベロープにつつまれている。エンベロープには２種類のスパイクすなわちhemagglutinin（HA）およびneuraminidase（NA）が独立して突き出ており，M2とよばれる蛋白も膜に存在する。A型インフルエンザウイルスは，その表面抗原が変異するため，しばしば大流行を起こし問題となる（**図8.2**）。

(2) 感染成立の機序

インフルエンザウイルスが細胞に対して感染性を発現するためには，HA蛋白がプロテアーゼ（蛋白分解酵素）によって，特定の１ヵ所で２つの蛋白サブユニット（HA1とHA2）とに分解される必要がある。宿主細胞に適当なプロテアーゼが存在するか否かによって，その組織でインフルエンザが感染巣を拡大できるか否か，その結果として病原性を発現するか否かが規定されることになる。

細胞内に取り込まれたウイルスは弱酸性の環境下でエンドソームと膜融合をおこし，M2蛋白のイオンチャンネル活性のもとエンベロープがもつ核様構造が解体され，裸のヌクレオカプシドが細胞質に放出され，ウイルスの増殖につながる。

増殖した感染細胞内ウイルスは，NA蛋白の酵素作用によりウイルスからシアル酸が切断分離され感染細胞から遊離し，宿主の他の細胞へ感染したり，体外へ咳嗽とともに排出される。

(3) 症状および臨床経過

インフルエンザに感染すると，1～3日の潜伏期を経て，悪寒戦慄，38度以上の発熱，頭痛，関節痛，全身倦怠感などの症状で発症し，続いて咳や鼻水などの呼吸器症状も目立ってくる。普通の風邪と異なる特徴は，呼吸器症状よりもむしろ全身症状が強く，重症感を伴うことで数日間は寝込むことも多い。このような症状を示して，約9割以上は1週間程度で回復する。

発症後3～4日間がウイルス排泄のピークで，他者への感染源となる。乳幼児がインフルエンザに初感染した場合には一般に症状は強く，ウイルス排泄量や排泄期間は長くなる。一方，高齢者では，しばしば発熱や自覚症状は軽度であるが，傾眠傾向を示したり，肺炎を合併[17]して死亡する例もみられる。

(4) 診断および治療

インフルエンザの診断は，数年前までは臨床症状以外には発病期と回復期のペア血清による抗体価上昇の確認，あるいは咽頭ぬぐい液などからのウイルス分離しかなく，臨床的な意義は少なかった。しかし，近年臨床の現場で，簡単にしかも短時間に診断可能な迅速診断キットが開発され，抗インフルエンザ薬であるノイラミニダーゼ阻害薬の開発とあいまって，インフルエンザの臨床は飛躍的に進歩した。

迅速診断キットは，イムノクロマト法あるいはEIA法を原理とし，特別な部屋および装置は必要なく，患者の鼻・咽頭ぬぐい液を検体として10－20分と短時間でA型，B型の型別診断まで可能で，感度80%以上，特異度90%以上である[18]。感度の低い理由として，検体採取が不十分な場合と，インフルエンザ初発日の検出率が第2および第3病日に比較して低いことである。これは感染者におけるウイルスの増殖と関連していると考えられる。

治療については上述したノイラミニダーゼ阻害薬およびアマンタジンが使用されている。ノイラミニダーゼ阻害薬は，NA蛋白の酵素作用を阻害しウイルスからシアル酸が切断分離されないようにし，ウイルス粒子を凝集させる。吸入薬のザナミビルと経口薬のオセルタミビルがあり，A型およびB型のいずれにも有効であり，副作用も少ない。アマンタジンと異なり耐性ウイルスはないとされていたが，最近，小児でオセルタミビル耐性ウイルスが出現したとの報告がある。アマンタジンはM2蛋白のイオンチャンネル作用を阻害することによりウイルスの増殖を抑制する。安価であるがA型にしか効果がなく，不眠，うつなどの中枢神経系副作用，あるいは悪心，食欲不振などの消化器系副作用がみられることがある。また，アマンタジン耐性ウイルスの出現も報告されている[19]。

(5) 一般的な感染予防

現在のところ，インフルエンザワクチンの接種が最も効果があるとされている。ワクチン接種が強く推奨されているハイリスク群としては，65歳以上の高齢者，老人ホームの居住者，慢性呼吸器・心血管系疾患患者および慢性代謝性，腎疾患などの免疫低下が考えられる患者，長期のアスピリン投与のためインフルエンザによるReye症候群の危険性が高い小児（生後6ヵ月から18歳），などが考えられる。

(6) 院内感染対策

医療従事者は自分が感染する危険性よりも，自分が感染して感染源となることを考慮し，ワクチン接種をするべきと考えられる。また，病棟内でインフルエンザが発症した場合，飛沫予防策でよいとの見解もあるが，咳嗽，くしゃみなどによりウイルスが飛沫核となって拡散することも考えられるため，空気予防策をとるべきでないかと考えられる。すなわち院内でインフルエンザが発生した場合，患者は個室隔離あるいはコホーテイングにて管理し，医療従事者は診療に際しては抗ウイルス対策用マスクを装着する。

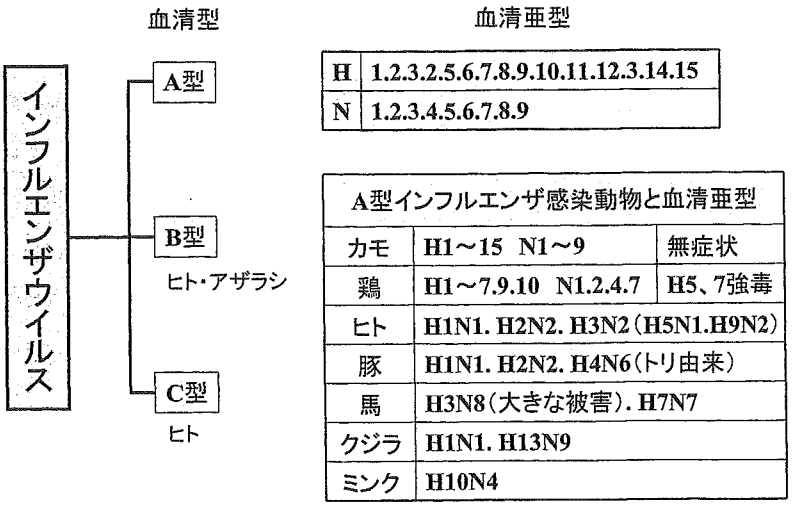

■ 図8.3. インフルエンザウイルスの分類と亜型 ■

(7) 高病原性鳥インフルエンザ (H5N1)

A型インフルエンザは表面抗原が変異することが知られ，今までヒトの世界で流行したインフルエンザはすべて鳥インフルエンザがヒトに感染し流行したものである。HA蛋白は1－15およびNA蛋白は1－9の亜型が存在し，その組み合わせで流行が起こっている。しかし，A型インフルエンザはカモなどの水鳥を中心にヒト，ウマ，ブタ，アザラシ，クジラ，ニワトリなどを自然宿主として増殖しながら，自然界に維持されている。特にカモは無症状で，その腸管にすべての亜型のHAとNAが組み合わされたさまざまなA型インフルエンザウイルスが感染している。このうちH5およびH7がニワトリには高病原性であり，感染すると100%死亡する（図8.3)。

1997年に香港でニワトリに小流行がみられ，ヒトへの感染もみられた（17名感染，5名死亡）A型インフルエンザ（H5N1）が，2004年からベトナムやタイで大流行しており，ニワトリだけでなく，ニワトリからヒトへ，さらにはヒトからヒトへの感染も認められ，死亡率が高いこともあり重大な問題となっている[20]。このウイルスの特徴として，インフルエンザワクチンはニワトリの受精卵を用いることから，高病原性鳥インフルエンザのワクチンを製造することが困難なため，その予防法としては一般にいわれているマスク，うがい，手洗いしかないのが現状である。しかし，治療に関してはノイラミニダーゼ阻害薬の早期投与で効果が確認されている。

いずれにしろ，このウイルスがヒトからヒトへ感染している事実を考えると，人間社会での大流行に注意する必要がある。

■2. 重症急性呼吸器症候群

(severe acute respiratory syndrome：SARS)

(1) 特徴

コロナウイルス粒子は，直径100－120nmの球形でエンベロープがあり，ウイルス粒子内に27～32kbのプラス1本鎖RNAをゲノムとして持つ。エンベロープにはM蛋白（membrane glycoprotein）とE蛋白（envelope protein）が存在し，粒子形成に重要な役割を果たしている。粒子表面の特徴的な20nmほどのスパイクはS蛋白（spike glycoprotein）からなっている。このスパイク構造があたかも王冠（crown，ラテン語でcorona）に見えるためコロナウイルスと命名された。S蛋白は細胞への吸着・結合・侵入に主要な役割を果たしている。

(2) 臨床症状および経過，治療

高熱（100%）と全身倦怠感（19－70%），筋肉痛（45－68%）など症状で発症し，水様性下痢（20－70%）もみられる。3日目から胸部X線上に肺炎陰影がみられ，10日目前後に肺炎の重症化と高度な低酸素血症が出現し，病状はピークに達する[21]。このピークは気道におけるウイルス量のピーク時期とほ

ぼ一致している。Choiら[22]は予後予測因子は60歳以上の年齢と，発症時の血清LDHの高値であると報告している。

治療法は確立されておらず，SARSコロナウイルスに特異的に効く薬剤はないが，臨床的にステロイドの大量投与が有効であったとの報告もある。実験的にはグリチルリチン，インターフェロン，抗HIV薬のプロテアーゼ阻害薬の一つであるネルフィナビルが有効であるとされている。

(3) 院内感染対策

SARSは院内感染によって感染が拡大した。したがって，院内感染対策を確実に行えば感染の拡大を防止できるものと考えられる。院内感染対策としては，インフルエンザの稿で述べた，空気感染予防策はもちろんのこと，気道分泌物だけでなく，便，尿，血液にもウイルスが排泄されているため[21]，接触感染予防策，さらには針刺しや血液検体の取り扱いにも注意する標準予防策の厳守も必要である。

ウイルスは発病後10～14日頃に排泄がピークとなっており，この時期は多くの症例が入院している時期であり院内で感染を起こしやすい（表8.1）。逆に，感染初期あるは症状が軽く日常生活を行っているヒトからはウイルスの排泄が少なく，他人へ感染させることは少ないと考えられた。また，SARS患者が入院した病院で，発熱や呼吸器症状がみられた医療従事者ではSARSに対する抗体の上昇や，気道分泌物からウイルスが分離されたが，症状のなかった職員ではこのような所見は得られなかったとの報告もある[23]。

■ 表8.1．インフルエンザとSARSの比較 ■

	インフルエンザ	SARS
感染性	初期に高い	発病4日以降に高い
ウイルス増殖	2日目にピーク	10日目にピーク
ウイルス排出	気道(6～8日)	気道(1～42日) 便(5～70日)
罹病期間	3～7日	2週間以上
肺炎発症頻度	9～25%	>90%
(肺炎による) 致命率	<1%	9.6%

■3．消化器系ウイルス感染症

消化器系ウイルス感染症は院内感染としてしばしば問題となることが多い。原因ウイルスとしては，アデノウイルス，エンテロウイルス，ロタウイルス，ノロウイルスなどがあるが，その確定診断法は便からのウイルス分離あるいはPCR法によるしかない。そのため，その院内感染対策としては患者の症状を目安にせざるを得ないことが多い。いずれにしても，院内感染対策としては接触感染予防策を行わなければならない。ここでは感染力が強いことから，注目されているノロウイルス感染症について述べる。

ノロウイルスはカリシウイルス科の中の一つで，代表するウイルス種はノーウォークウイルス（Norwalk virus）である。現時点では，ノロウイルス属に入るウイルス種はノーウォークウイルスのみである。

ノロウイルスは正20面体で直径27－35nmの小型ウイルスである。エンベロープはなく，遺伝子はプラス鎖の1本鎖RNAである。感染様式は糞口感染である。発症後少なくとも1週間は糞便中にウイルスが排出され感染源となる。ノロウイルスでは，こういったヒトからヒトへの感染以外に，汚染された飲料水や食物（生カキが最も多い）からの感染があり，ウイルス性食中毒の集団発生の原因となる。

臨床症状としては，発熱，嘔吐，下痢，腹痛で，特に嘔吐の頻度が高い傾向にある。ウイルスは糞便中に1週間は排泄され感染源となりえる。ノロウイルス胃腸炎は通年性にみられるが，わが国における好発季節は11月から1月にピークがあり[24]，その後，ロタウイルス胃腸炎のピークが1月から4月にかけてみられる[25]。

治療としては，輸液などにより下痢による脱水の改善を図る。近年，高齢者の死亡報告もあり注意を要する。

■4．発疹性ウイルス感染症

これらのウイルス感染症は，主として小児期の感染症であるが，若年成人での感染が増加しており，臨床上および院内感染対策上重要な問題となってい

る。麻疹ウイルスは直径200nmのRNAウイルスで，感染すると10～12日の潜伏期間後に，発熱，結膜充血，風邪症状などのカタル期を経て，全身性に発疹が出現し，10日前後で回復する。成人麻疹は肺炎などの合併や[26]，一過性の強い免疫抑制状態になり重症化することがある。

わが国での問題は，この重症化する成人麻疹が増加していることである。この理由としては，病後免疫およびワクチン接種後免疫は麻疹の再感染を受け，不顕性感染を繰り返すことで自然追加免疫の効果が得られ結果的に免疫が長期間持続している[27]。しかし，近年，麻疹の流行が小規模になり，不顕性感染の機会が減少するため，病後免疫もワクチン接種後の免疫も減弱する。このため再感染を受けたとき発病を免れることができない成人が増加しているためと考えられる。予防としては麻疹ワクチンしかないが，ワクチンによる獲得免疫は終生免疫ではないことは理解しておかなければならない。

風疹ウイルスは，直径60－70nmのRNAウイルスである。風疹は21日の潜伏期間の後に発熱，淡いピンク色の発疹，耳介後部から頚部にかけてリンパ腺腫脹が出現するが，3日くらいで治るため，子供の軽いウイルス感染症と考えられている。しかし，妊娠初期の女性が感染すると，生まれてきた子供の20%は白内障，心奇形，難聴などの先天異常をきたすため，重要なウイルス感染症の一つである。このため母体の風疹感染を理由とする人口流産が増加し，わが国の少子化問題に拍車をかけている。予防方法は風疹ワクチンの接種である。

院内感染対策としては，麻疹は空気感染予防策で，風疹は飛沫予防策である。

おわりに

ウイルス感染症は，近年，診断および抗ウイルス薬の開発とともに制御しやすい疾患となってきてはいるが，空気感染などにより流行すると拡大しやすいウイルスや，持続感染を起こし慢性疾患の原因となったり，感染源となったりするウイルスもあり，治療だけでなく，他人への感染防止を考えた十分な対応が必要と考えられる。

参考文献

1) Furusyo N, Nakashima H, Kashiwagi K, et al. : Clinical outcomes of hepatitis B virus (HBV) genotypes B and C in Japanese patients with chronic HBV. Am J Trop Med Hyg, **67**:170-175, 2002.
2) Hayashi J, Kashiwagi S, Nomura H, et al. : Hepatitis B virus transmission in nursery schools. Am J Epidemiol, **125**:492-498, 1987.
3) Furusyo N, Hayashi J, Sawayama Y, et al. : The elimination of hepatitis B virus infection: Changing seroepidemiology of hepatitis A and B virus infection in Okinawa, Japan over a 26 year period. Am J Trop Med Hyg, **59**:693-698, 1998.
4) Hayashi J, Kashiwagi S, Okeda T, et al. : Electrocardiographic changes induced by hypersecretion of catecholamine in the patient with fulminant hepatitis. J J Med, **27**:187-190, 1988.
5) Furusyo N, Takeoka H, Toyoda K, et al. : Long-term lamivudine treatment of chronic hepatitis B in Japanese patients: A project of the Kyushu University Liver Disease Study. World J Gastroenterol (in press)
6) 林　純, 柏木征三郎, 池松秀之ほか：医療従事者におけるHBワクチン接種後の長期観察と追加接種について. 感染症誌, **62**:805-810, 1988.
7) Hayashi J, Kashiwagi S, Nomura H, et al. : The control of hepatitis B virus infection with vaccine in Japanese nursery schools. Am J Epidemiol, **126**:474-479, 1987.
8) Hayashi J, Kashiwagi S, Noguchi A, et al. : Intradermal hepatitis B vaccination for mentally retarded patients. J Infect, **19**:119-125, 1989.
9) 林　純, 古庄憲浩, 中牟田誠ほか：HBs抗原消失の機序とその後の問題点. 日本臨床, **62**増刊 8,106-111, 2004.
10) Hayashi J, Nakashima K, Kajiyama W, et al. : Prevalence of antibody to hepatitis C virus in hemodialysis patients. Am J Epidemiol, **134**:651-657, 1991.
11) Hayashi J, Kishihara Y, Yamaji K, et al. : Transmission of hepatitis C virus by health care workers in a rural area of Japan. Am J Gastroenterol, **90**:794-799, 1995.

12) Hayashi J, Hirata M, Nakashima K, et al. : Hepatitis C virus is a more likely cause of chronic liver disease in the Japanese population than hepatitis B virus. Fukuoka Acta Med, **82**:648-654, 1991.
13) Hayashi J, Ohmiya M, Kishihara Y, et al. : A statistical analysis of predictive factors of response to humanl ymphoblastoid interferon in patients with chronic hepatitis C. Am J Gastroenterol, **89**:2151-2156, 1994.
14) Hayashi J, Frusyo N, Ariyama I, et al. : A relationship between the evolution of hepatitis C virus variants, liver damage, and hepatocellular carcinoma in patients with hepatitis C viremia. J Infect Dis, **181**:1523-1527, 2000.
15) Nakashima K, Kashiwagi S, Hayashi J, et al. : Sexual transmission of hepatitis C virus among female prostitutes and patients with sexually transmitted diseases in Fukuoka, Kyushu, Japan. Am J Epidemiol, **136**:1132-1137, 1992.
16) Nomura H, Sou S, Nagahama T, et al. : Short-term interferon-alfa therapy for acute hepatitis C: A randomized controlled trial. Hepatology, **39**: 1213-1219, 2004.
17) 中嶋　寿, 山本哲郎, 岸原康浩ほか：画像上インフルエンザウイルス肺炎が疑われ、CPK高値が認められたA型インフルエンザの１症例. 臨床と研究, **76**: 2163-2166, 1999.
18) 久保徳彦, 池松秀之, 鍋島茂樹ほか：イムノクロマトグラフィーを原理としたインフルエンザ迅速診断キットの成人における有用性についての検討. 感染症誌, **77**: 1007-1014, 2003.
19) 柏木征三郎：抗インフルエンザ薬の効果. 臨床と研究, **79**: 2075-2079, 2002.
20) Tran TH, Nguyen TL, Nguen TD, et al. : Avian influenza A (H5N1) in 10 patients in Vietnam. N Engl J Med, **350**: 1179-1188, 2004.
21) Peiris JS, Chu CM, Cheng VC, et al. : Clinical progression and viral load in a community outbreak of coronavirus-associated SARS pneumonia: a prospective study. Lancet, **361**: 1767-1772, 2003.
22) Choi KW, Chau TN, Tsang O, et al. : Outcomes and prognostic factors in 267 patients with severe acute respiratory syndrome in Hong Kong. Ann Intern Med, **139**: 715-723, 2003.
23) Ho KY, Singh KS, Habib AG, et al. : Mild illness associated with severe acute respiratory syndrome coronavirus infection : lessons from a prospective seroepidemiologic study health-care workers in a teaching hospital in Singapore. J Infect Dis, **189**: 642-647, 2004.
24) Nakata S, Honma S, Numata KK, et al. : Members of the family caliciviridae (Norwalk virus and Sapporo virus) are the most prevalent cause of gastroenteritis outbreaks among infants in Japan. J Infect Dis, **181**:2029-2032, 2000.
25) Inoue S, Yamashita K, Yamadera S, et al. : Surveillance of viral gastroenteritis in Japan. Pediatric cases and outbreak incidents. J Infect Dis, **181**:S 270-272, 2000.
26) 達川政文, 澤山泰典, 鍋島茂樹ほか：ステロイドパルス、ビタミンA大量及びγグロブリンの併用療法が有効であった成人麻疹肺炎の1症例. 感染症誌, **75**：989-993, 2001.
27) 中山哲夫：麻疹の流行と対策. モダンメディア, **48**: 55-57, 2002.

0021-972X/05/$15.00/0
Printed in U.S.A.

The Journal of Clinical Endocrinology & Metabolism 90(11):6162–6169
Copyright © 2005 by The Endocrine Society
doi: 10.1210/jc.2005-0179

Impaired Nuclear Translocation, Nuclear Matrix Targeting, and Intranuclear Mobility of Mutant Androgen Receptors Carrying Amino Acid Substitutions in the Deoxyribonucleic Acid-Binding Domain Derived from Androgen Insensitivity Syndrome Patients

Hisaya Kawate, Yin Wu, Keizo Ohnaka, Rong-Hua Tao, Kei-ichiro Nakamura, Taijiro Okabe, Toshihiko Yanase, Hajime Nawata, and Ryoichi Takayanagi

Departments of Geriatric Medicine (H.K., Y.W., K.O., R.-H.T., R.T.) and Medicine and Bioregulatory Science (T.O., T.Y., H.N.), Graduate School of Medical Sciences, Kyushu University, Fukuoka 812-8582, Japan; and Department of the Second Anatomy (K.N.), Kurume University School of Medicine, Kurume, 830-0011, Japan

Context: Recent imaging studies revealed that androgen receptor (AR) is ligand-dependently translocated from the cytoplasm into the nucleus and forms intranuclear fine foci. In this study, we examined whether intracellular dynamics of mutant ARs detected in two androgen insensitivity syndrome (AIS) patients was impaired.

Objective: ARs with mutations in the DNA-binding domain were functionally characterized and compared with the wild-type AR.

Patients: In a complete AIS patient (subject 1), cysteine residue 579 in the first zinc finger motif of AR was substituted for phenylalanine (AR-C579F). Another mutation (AR-F582Y) was found in a partial AIS patient (subject 2).

Results: AR-F582Y retained less than 10% of the transactivation activity of the wild-type AR, whereas no ligand-dependent transactivation was detected for AR-C579F. Image analyses of the receptors fused to green fluorescent protein showed that the wild-type AR was ligand-dependently translocated into the nucleus in which it formed fine subnuclear foci. Surprisingly, after the addition of dihydrotestosterone, the two mutant ARs initially formed large cytoplasmic dots, many of which were found to be close to mitochondria by electron microscopy. Subsequently, a part of the ligand-bound mutant ARs gradually entered the nucleus to form a smaller number of larger dots, compared with the wild-type AR. Fluorescence recovery after photobleaching analysis revealed that the intranuclear mobility of the mutant ARs decreased, compared with that of the wild-type AR.

Conclusions: These results suggest that the abnormal translocation, localization, and mobility of the mutant ARs may be the cause of AIS in these subjects. (***J Clin Endocrinol Metab* 90: 6162–6169, 2005**)

ANDROGENS PLAY AN essential role in the expression of the male phenotype. The actions of androgens are mainly mediated by the androgen receptor (AR). The AR belongs to the nuclear receptor superfamily, a large group of transcription factors whose members share basic structural and functional homology (1, 2). The N-terminal domain of the AR contains the major transactivation function region, AF-1, which acts in a ligand-independent fashion. The centrally located DNA-binding domain (DBD) is highly conserved among steroid hormone receptors and consists of two zinc finger clusters. The first zinc finger motif is involved in direct DNA-binding and contains the P-box for specific recognition of the androgen-responsive elements of target genes (3). The C-terminal ligand-binding domain (LBD) contains transactivation function domain 2 and functionally interacts with intermediary factors and nuclear cofactors. In the absence of an agonist, the LBD is believed to prevent the transactivation function of the N-terminal domain through an intramolecular interaction (4).

Unliganded ARs are located in the cytoplasm, in which they are sequestered with heat shock proteins. After ligand binding, a conformational change of the receptor protein results in unmasking of both the dimerization motif and the nuclear localization signal that allows translocation into the nucleus (1). Upon nuclear entry, the ligand-receptor complexes appear to move into subnuclear compartments, which are common congregation sites for steroid hormone receptors and other associated factors, such as nuclear receptor coactivators, that are required for transcriptional activation of the target genes. Complete subnuclear foci formation seems to be essential for steroid hormone receptor-mediated transactivation (4–6).

Because the human AR gene is located on the X chromosome at Xq11–12 (1, 4, 7), just a single allele mutation in the AR gene causes dysfunction of the receptor in 46, XY individuals, resulting in androgen insensitivity syndrome (AIS) (3, 8–10). Despite a high or normal level of serum testoster-

First Published Online August 23, 2005

Abbreviations: AIS, Androgen insensitivity syndrome; AR, androgen receptor; CAIS, complete androgen insensitivity syndrome; 3D, three-dimensional; DBD, DNA-binding domain; DHT, dihydrotestosterone; FBS, fetal bovine serum; FRAP, fluorescence recovery after photobleaching; GFP, green fluorescent protein; GR, glucocorticoid receptor; LBD, ligand-binding domain; PAIS, partial androgen insensitivity syndrome; $t_{1/2}$, half-recovery time; YFP, yellow fluorescent protein.

JCEM is published monthly by The Endocrine Society (http://www.endo-society.org), the foremost professional society serving the endocrine community.

one, AIS patients show various phenotypic abnormalities of male sexual development. AIS is subdivided into three phenotypes: complete androgen insensitivity syndrome (CAIS), partial androgen insensitivity syndrome (PAIS), and mild androgen insensitivity syndrome. AR mutations that severely impair the function of the AR cause CAIS. The main phenotypic characteristics of individuals with CAIS are female external genitalia with a short, blind-ending vagina, absent Müllerian duct, and absence of pubic and axillary hair. The gender identity is that of a normal female, but testes are commonly located in either the abdomen or the inguinal area and the uterus is absent. Laboratory findings show the 46, XY karyotype, normal or increased synthesis of testosterone by the testes, and a normal or increased level of LH. PAIS patients also show female-like external genitalia, except for clitoromegaly and/or posterior labial fusion (3, 9). Although mutations responsible for AIS are spread throughout the AR gene, there are hot spots, especially at exon 5, which encodes part of the LBD (Androgen Receptor Gene Mutation Database: www.mcgill.ca/androgendb).

We previously reported two unrelated AIS patients (one CAIS and one PAIS) carrying amino acid substitutions in the first zinc finger motif of the AR-DBD (11). In the CAIS patient (subject 1), cysteine residue 579, which coordinates a zinc ion, was substituted with phenylalanine, and the mutant AR showed almost no ligand-induced transcriptional activation. On the other hand, the AR-F582Y mutant found in the PAIS patient (subject 2) showed much less transactivation than the wild-type AR. Here, to visualize any dynamic changes of the intracellular localizations of these mutant ARs, the wild-type and mutant ARs were fused with green fluorescent protein (GFP) and their intracellular movements were analyzed using a laser confocal microscope. After treatment with the ligand, the wild-type AR was translocated from the cytoplasm into the nucleus in which it formed fine subnuclear foci. In contrast, the AR-DBD mutants initially formed large cytoplasmic dots, many of which were located close to mitochondria after the addition of dihydrotestosterone (DHT), and a proportion of the proteins subsequently moved into the nucleus to become located in subnuclear bodies. The subnuclear foci of the mutant ARs were characterized by their larger size, much smaller number, and lower mobility, compared with the wild-type AR. These results indicate that the pathogenesis of AIS in these two patients may be caused by the mislocation and lower mobility of their mutant ARs.

Subjects and Methods

Subjects

Subjects 1 and 2 were diagnosed with CAIS and PAIS, respectively, and had missense mutations of Cys^{579} to Phe and Phe^{582} to Tyr, respectively. The clinical history and data of the AIS patients characterized in the present study were previously reported (11).

Cells

COS-7 monkey kidney cells were obtained from the Riken Cell Bank (Tokyo, Japan) and maintained in DMEM (Invitrogen, Carlsbad, CA) containing antibiotics and 10% fetal bovine serum (FBS; Cansera International Inc., Etobicoke, Canada).

Plasmids

The firefly luciferase reporter plasmids, pGL3-MMTV (5) and pGL3-PSA (12), and the expression vectors for AR (pCMV-AR) were prepared as previously described (13, 14). The plasmid vectors pAR-GFP (5) and pAR-CFP (6) for expression of the AR-GFP and AR-CFP fusion proteins were constructed as described previously. Expression plasmids of the mutant ARs for mammalian cells, designated pCMV-AR-C579F (from subject 1) and pCMV-AR-F582Y (from subject 2), were constructed as previously reported (11). To construct a GFP fusion protein of the mutant AR for subject 1, a *Kpn*I-*Sca*I fragment of pCMV-AR-C579F, which contained the mutated site, was replaced with that of pAR-GFP to generate pAR-C579F-GFP. Similarly, for subject 2, a *Hin*dIII-*Sca*I fragment of pAR-GFP was replaced with that of pCMV-AR-F582Y to construct pAR-F582Y-GFP. The validity of the structure of each construct was confirmed by DNA sequencing using an ABI PRISM 377 DNA sequencer (Applied Biosystems, Foster City, CA).

Immunoblotting

COS-7 cells were seeded in 100-mm plates and incubated for 24 h in 5% CO_2 at 37 C. Five micrograms of plasmid DNA carrying the wild-type or a mutant AR was transfected into the cells using 20 μl Superfect transfection reagent (QIAGEN GmbH, Hilden, Germany). Twenty-four hours after the transfection, the cells were washed twice with PBS and then 400 μl of Nonidet P-40 lysis buffer [50 mM Tris-HCl (pH 8.0), 150 mM NaCl, and 1% Nonidet P-40] was added to each dish, followed by rocking for 30 min at 4 C. Lysates were collected by centrifugation and the protein concentrations were measured using a BCA protein assay kit (Pierce, Rockford IL). Next, 40 μg of each lysate in 1× SDS-PAGE sample buffer [2% sodium dodecyl sulfate, 100 mM dithiothreitol, 60 mM Tris-HCl (pH 6.8), and 0.01% bromophenol blue] was loaded onto a sodium dodecyl sulfate-polyacrylamide gel (10% separating gel) and electrophoresed at 20 mA for 4 h. Proteins were transferred onto nitrocellulose membrane (Hybond P; Amersham Biosciences, Piscataway, NJ) using a Trans-Blot SD Semi-Dry transfer cell (Bio-Rad Laboratories, Hercules, CA) at 250 V for 1 h at 25 C. After blocking the membrane in 1× Block-Ace (Dainippon Pharmaceutical Co., Osaka, Japan), an anti-AR polyclonal antibody (sc-816; Santa Cruz Biotechnology Inc., Santa Cruz, CA) was reacted with the membrane in 0.1× Block-Ace for 1 h at 25 C. After a brief wash with Tris-buffered saline-Tween 20 (10 mM Tris-HCl, 0.9% NaCl, and 0.05% Tween 20), horseradish peroxidase-conjugated antirabbit Ig antibodies (Amersham Biosciences) were added in 0.1× Block-Ace as the secondary antibody, and the membrane was incubated for 45 min at 25 C with gentle shaking. After washing with Tris-buffered saline-Tween 20, the membrane was reacted with Western blotting detection reagents (Amersham Biosciences) for 1 min in a dark room. The labeled protein bands were visualized and analyzed using a VersaDoc imaging system 5000 (Bio-Rad).

Functional reporter assays

COS-7 cells (1 $\times 10^5$ cells/well) were seeded in 12-well plates at 20 h before transfection. Cells were cotransfected with 0.5 μg/well of pGL3-MMTV as a reporter plasmid, 2 ng/well of pRL-CMV (Promega Corp., Madison, WI) as an internal control, and 0.1 μg/well of a wild-type or mutant AR expression plasmid with 1.7 μl/well of Superfect. In all transfection experiments, the total amount of plasmid DNA was fixed by adding empty vector to the transfection mixture. At 3 h after transfection, 0.5 ml of DMEM containing 10% charcoal-treated FBS was added with or without steroid hormone (10^{-8} M DHT). After incubation for 24 h, the cells were rinsed with PBS and lysed in the lysis buffer contained in a luciferase assay kit (Promega). The luciferase activity was assayed using the dual-luciferase assay system (Promega) and a Lumat LB 9507 (Berthold Technologies, Bad Wildbad, Germany). Each value was determined as the average of three independent experiments. Data were presented as the means ± SD. One-way ANOVA followed by Scheffé's test was used for multigroup comparisons. $P < 0.05$ was considered to be statistically significant

Confocal laser-scanning microscopy

For living cell microscopy, COS-7 cells (2 $\times 10^5$ cells/well) were seeded in 35-mm glass-bottom dishes (Asahi Techno Glass Corp., Tokyo,

Japan) and transfected with 0.5 μg of plasmid DNA carrying the wild-type or a mutant AR fused with GFP or yellow fluorescent protein (YFP) using 5 μl/well Superfect. The cells were maintained in DMEM supplemented with 10% charcoal-treated FBS for 20 h, and then various steroid hormones were added to the medium. The cells were observed with an Axiovert 200M inverted microscope equipped with an LSM510META scan head (Carl Zeiss, Jena, Germany) using a ×100, 1.4 numerical aperture oil immersion objective. Images were collected at a 12-bit depth resolution of intensities over 1024 × 1024 pixels. For excitation of GFP and YFP, a 488-nm argon laser was used and a series of images was obtained. The GFP and YFP signals were separated using the emission fingerprinting technique established by Carl Zeiss. Separation of the individual emission signals was based on recording a spectral signature and applying a linear unmixing algorithm using the reference spectra of each fluorescent protein (15).

To construct three-dimensional (3D) images, a series of 30–50 two-dimensional tomographic images were collected for each cell using the confocal microscope. These images were exported as TIF files and the TRI graphic program (Ratoc System Engineering, Tokyo, Japan) was used to reconstruct 3D images (6). Both the spatial distribution and calculation of the fluorescent proteins as distinct volumes were made possible by removing scattering background fluorescence and lens spherical aberrations and then separating each particle (6). The numbers of subnuclear foci determined for the wild-type and mutant ARs were representative of at least 20 cells.

Fluorescence recovery after photobleaching (FRAP) analysis

Cells were transfected with the wild-type AR and a mutant AR and incubated for 24 h at 37 C. After a further 5-h incubation with DHT, FRAP analysis was performed. After collection of the initial image using a Carl Zeiss LSM510META microscope, a selected area of a fixed size in the nucleus was photobleached by setting the laser wavelength to 488 nm and using the maximum power for 50 iterations. After the bleaching, images within the bleached region were taken every second at a resolution of 512 × 512 pixels to follow the recovery of the fluorescence intensity. The intensity of the fluorescence was calculated using the LSM510 software and the half-recovery time ($t_{1/2}$) was determined as the time when the fluorescence intensity reached half the maximal recovery using the Microsoft Excel software. Each $t_{1/2}$ was the average of six to 10 FRAP experiments.

Organelle detection

COS-7 cells were transfected with pAR-C579F-GFP. Twenty-four hours after the transfection, the cells were treated with DHT and then LysoTracker Red or MitoTracker Orange CMTMRos (Molecular Probes Inc., Eugene, OR) was added in the medium at a final concentration of 100 nM to visualize the lysosomes or mitochondria, respectively. The cells were incubated for 30 min at 37 C and then rinsed with PBS. Images were collected using the fluorescence microscope.

Immunoelectron microscopy

Twenty-four hours before transfection, COS-7 cells were seeded in a 60-mm dish. The cells were transfected with 2 μg of pAR-C579F-GFP using 3 μl of Superfect. After incubation for 20 h, the cells were treated with 10^{-8} M DHT for 1 h. After a brief wash with PBS, the cells were fixed in 0.1% glutaraldehyde in 0.1 M phosphate buffer (pH 7.4) for 30 min at 25 C. The fixed cells were scraped off the dish, centrifuged at 5000 × *g* for 10 min at 4 C and resuspended in 0.1 M phosphate buffer. After dehydration in a graded series of ethanol, the cell pellet was embedded in LR White resin and ultrathin sections were cut (16). After blocking in 0.1 M phosphate buffer containing 3% BSA, the sections were incubated with rabbit polyclonal antibodies against GFP (BD Biosciences Clontech, Mountain View, CA) at 1:1000 dilution in 0.1 M phosphate buffer at 4 C overnight, followed by incubation with colloidal gold (Ø = 15 nm)-conjugated goat antirabbit IgG (Amersham Biosciences) at 1:100 dilution. After washing with distilled water, the sections was stained with 2% uranyl acetate and lead citrate, and observed with a Hitachi H-7000 electron microscope (Hitachinaka, Japan).

Results

Previously we found two different amino acid substitutions in the DBD of ARs derived from AIS patients (11). One mutation from a CAIS patient (subject 1) occurred at Cys579 which coordinates a zinc ion in the first zinc finger motif of the AR (Fig. 1A). This residue also forms a P-box that is important for the recognition of an androgen-responsive element in target genes. The other mutation from a PAIS patient (subject 2) was found at Phe582 next to the P-box (Fig. 1A). To compare the functions of these two mutant ARs with the wild-type AR, recombinant AR proteins were expressed in COS-7 cells. Immunoblot analysis showed that the expression levels of the wild-type and mutant ARs in transfected cells were almost the same (Fig. 1B). To examine AR-mediated transcriptional activation, luciferase assays were performed using the MMTV promoter containing several hormone-responsive elements (17). For the wild-type AR,

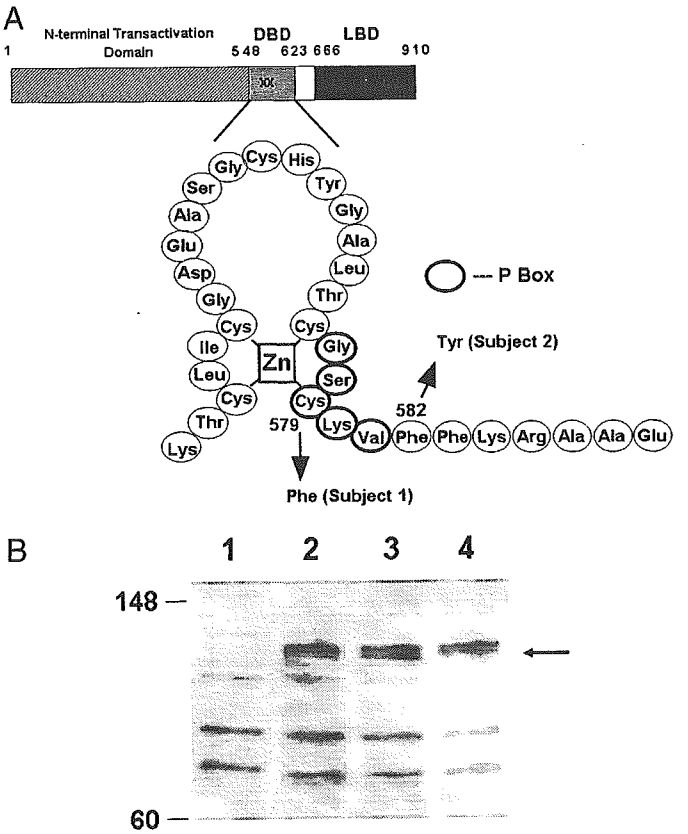

FIG. 1. The amino acid substitutions in the two AIS patients are located in the DBD of the AR. A, Schematic representation of the AR and the sites of the amino acid substitutions detected in the AIS patients. The *upper scheme* shows the domain structure of the AR: the N-terminal domain, the DBD, and the C-terminal LBD. Two different amino acid substitutions (x) were identified in the DBD of the ARs from these two AIS patients. The first zinc finger motif of the AR-DBD is magnified in the *lower scheme*. The five amino acids *circled in bold* indicate the P-box. The *arrows* indicate the amino acid substitutions in the two AIS patients. In subject 1, the cysteine at position 579 involved in the P-box is substituted by phenylalanine (C579F). In subject 2, phenylalanine 582 is changed for tyrosine (F582Y). B, Immunoblot analysis of wild-type and mutant ARs in COS-7 cells. Cells were transfected with a wild-type or mutant AR expression vector using Superfect. Twenty-four hours after the transfection, the cells were lysed and subjected to immunoblotting analysis as described in *Subjects and Methods*. Anti-AR antibodies were used for detection. The *arrow* shows the AR bands. Lane 1, Vector only; lane 2, wild-type AR; lane 3, AR-F582Y; lane 4, AR-C579F. The *numbers on the left* of the gel show the positions of protein size markers.

remarkable transcriptional activation was observed after addition of the ligand DHT. On the other hand, AR-F582Y showed less than 10% of the transcriptional activation of the wild-type AR, whereas AR-C579F showed no ligand-dependent transactivation at all (Fig. 2).

To visualize the subcellular localizations of the wild-type and mutant ARs, GFP-fusion proteins were generated and observed under a confocal laser-scanning microscope. As we previously reported, the wild-type AR was diffusely localized in the cytoplasm in the absence of the ligand (Fig. 3A) (5). Upon treatment with the ligand, the wild-type AR was almost completely translocated from the cytoplasm into the nucleus in which it formed subnuclear fine foci (Fig. 3D). The AR-DBD mutants were also diffusely present in the cytoplasm before addition of the ligand (Fig. 3, B and C). However, in contrast to the wild-type AR, the two mutant ARs formed cytoplasmic dots after the addition of DHT (Fig. 3, E and F). Time-course experiments revealed that most of the fluorescent signals for the wild-type AR were observed in the nucleus within 30 min after the addition of DHT (Fig. 4B), whereas cells expressing the AR-C579F mutant showed two patterns (Fig. 4, E–H or I–L). Approximately 80% of cells formed the cytoplasmic dots and a limited number of nuclear foci 30 min after the addition of DHT (Fig. 4F), and the nuclear dots became clear at 3 h after the ligand addition (Fig. 4H). In the other type of AR-C579F-expressing cells (20%), cytoplasmic dots were not so striking (Fig. 4J), but delayed nuclear translocation with dot formation of mutant AR was observed (Fig. 4L). In both types of the mutant-expressing cells, a smaller number of larger-sized intranuclear dots for

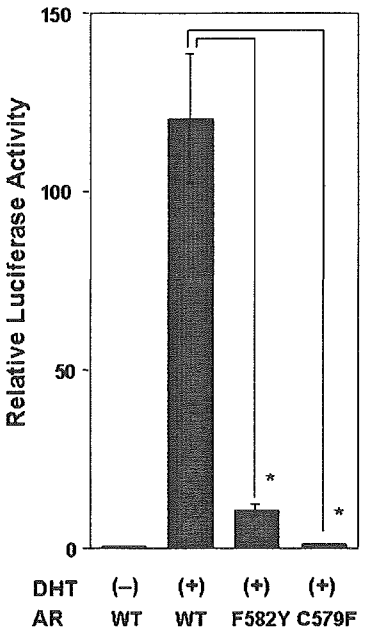

FIG. 2. Effects of the two different amino acid substitutions in the AR-DBD on transcriptional activation. COS-7 cells were transiently transfected with plasmid DNA expressing the wild-type (WT) or a mutant (C579F or F582Y) AR, pGL3-MMTV as a reporter plasmid, and pRL-CMV as an internal control. After treatment with or without 10^{-8} M DHT for 24 h, the luciferase activity was measured. The *bars* show the luciferase activities of the transfected cells relative to the value of the wild-type AR without DHT. The means ± SD of three independent experiments are shown. *, $P < 0.05$.

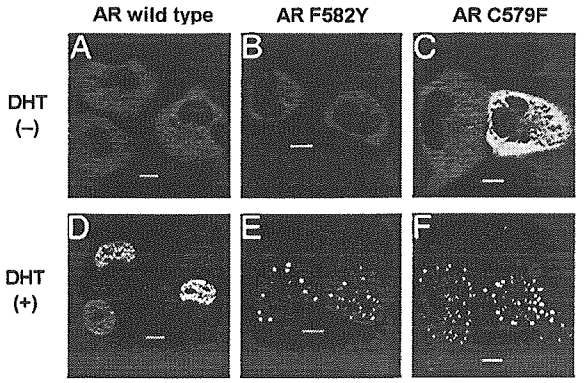

FIG. 3. Ligand-dependent translocation of the wild-type and mutant ARs. COS-7 cells were transfected with 0.5 μg of each plasmid DNA expressing GFP-fused wild-type AR (A and D), AR-F582Y (B and E), or AR-C579F (C and F). Fluorescent signals were observed at 24 h after the transfection under a laser confocal microscope (A–C). Subsequently 10^{-8} M DHT was added and incubated at 37 C for 1 h and the ligand-bound receptor proteins were observed (D–F). *Scale bar*, 10 μm.

AR-C579F were observed, compared with those for the wild-type AR (Fig. 4, D, H, and L). Even after a 3-h treatment with the ligand, a significant amount of the mutant AR still remained in the cytoplasm (Fig. 4, H and L), whereas almost all the signals for the wild-type AR were detected in the nucleus (Fig. 4D). These data indicate that the nuclear translocation and subnuclear localization are impaired in AR-DBD mutants.

To quantitatively analyze the subnuclear foci, 3D images were constructed from the tomographic images collected using the confocal microscope. As shown in Fig. 5, both the C579F and F582Y AR mutants had a much lower number of foci in the nucleus than the wild-type AR. The average number of nuclear foci for the wild-type AR was 300 ± 8, whereas the numbers for F582Y and C579F were 106 ± 18 and 127 ± 23, respectively.

To examine whether the mutant ARs inhibit the nuclear translocation of the wild-type AR, we cotransfected the wild-type AR fused to GFP (AR-WT-GFP) and AR-C579F-CMV (without GFP) and observed the cells under the confocal microscope. Cotransfection of AR-WT-GFP with AR-C579F-CMV showed cytoplasmic dots in addition to fine nuclear foci after treatment with DHT (Fig. 6Ab). Opposite experiments using AR-C579F-GFP and AR-WT-CMV led to similar results, revealing that both nuclear and cytoplasmic dots appeared after incubation with DHT (Fig. 6Ad). To confirm the colocalization of the wild-type and mutant ARs, AR-WT-CFP and AR-C579F-GFP were coexpressed, and each fluorescent signal was collected under the laser confocal microscope. As shown in Fig. 6B, wild-type and mutant ARs were colocalized in both the nuclear and cytoplasmic dots in the presence of 10 nM DHT (Fig. 6B, d–f). The magnitude of the transcriptional activation in the cells transfected with both AR-WT and AR-C579F was less than half that induced by AR-WT (Fig. 6C). In addition to this experiment using 10 nM DHT, we measured the transcriptional activation of the wild-type AR in the presence of 5 nM DHT. The reporter luciferase activity of the wild-type at 5 nM DHT was significantly higher than that by combination of the wild-type and

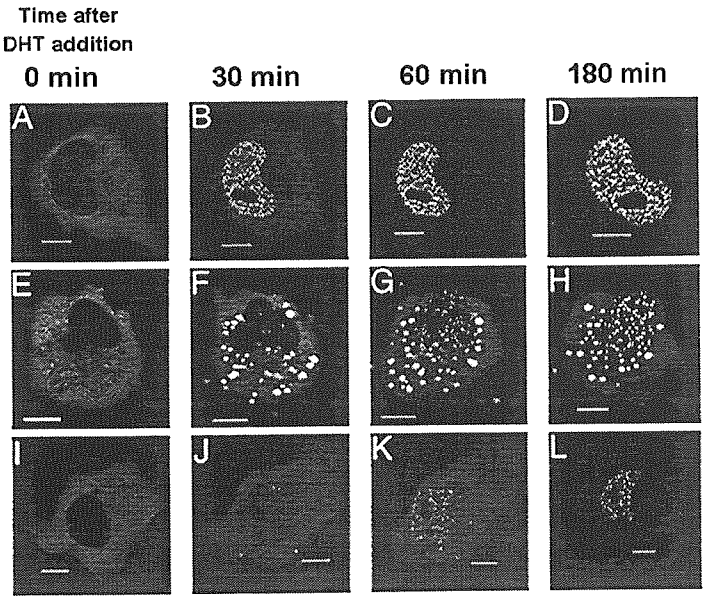

FIG. 4. Time-lapse translocation of wild-type (WT) and mutant ARs after the addition of DHT. COS-7 cells expressing wild-type AR (A–D) or the AR-C579F mutant (E–H and I–L) were treated with 10^{-8} M DHT. Images were collected using a laser confocal microscope before the DHT treatment (A, E, and I) and at 30 (B, F, and J), 60 (C, G, and K), and 180 min (D, H, and L) after the treatment. *Scale bar*, 10 μm.

AR-C579F at 10 nM. Even in a high dose of DHT (100 nM), which can fill all the wild-type LBD, coexpression of AR-C579F inhibited the transcriptional activation mediated by the wild-type AR (Fig. 6C). These results indicated that simple stealing of ligand by AR-C579F is not able to explain the suppression effect of AR-C579F and strongly suggested that AR-C579F is able to form heterodimers with AR-WT in the cells and inhibit the translocation of AR-WT, thereby reducing the transactivation.

As shown in Figs. 4 and 5, the numbers of nuclear foci for the mutant ARs were much lower than that for the wild-type AR. To evaluate whether there are any differences in dynamics between the nuclear foci of the wild-type and mutant ARs, the mobilities of the wild-type and mutant ARs in the nucleus were measured quantitatively by FRAP analysis. After a short period of photobleaching at the maximal power of the laser, continuous images were taken at 1-sec intervals. As shown in Fig. 7A, the recovery of the fluorescence intensity for AR-C579F foci was slower than that for AR-WT. The fluorescence recovery was evaluated by plotting the intensity of the bleached area against time (Fig. 7B). Compared with the wild-type AR, the slope of the fluorescence recovery of AR-C579F was relatively gentle. The $t_{1/2}$ for AR-C579F was 10.5 ± 1.6 sec (n = 12), which was significantly slower than

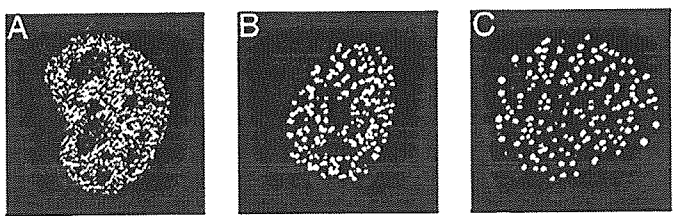

FIG. 5. Three-dimensional image analyses of the intranuclear foci of the wild-type and mutant ARs. COS-7 cells were transfected with 0.5 μg of pAR-GFP (A), pAR-F582Y-GFP (B), or pAR-C579F-GFP (C). Twenty-four hours after the transfection, the cells were treated with DHT and two-dimensional tomographic images collected using the confocal microscope were used to reconstruct 3D images as described in *Subjects and Methods*.

that for the wild-type AR [8.0 ± 1.1 sec (n = 10)]. In another experiment, AR-F582Y also showed reduced mobility, compared with the wild type [$t_{1/2}$ = 8.4 ± 1.1 sec (n = 6)], and the $t_{1/2}$ for AR-F582Y [9.9 ± 1.2 sec (n = 6)] was almost the same as that for AR-C579F [10.2 ± 1.1 sec (n = 6)]. These results indicate that the DBD amino acid substitution in the mutant AR caused decreased mobility of the AR in the nucleus.

As shown in Fig. 3, AR-DBD mutants showed ligand-dependent formation of large cytoplasmic dots. We investigated the localizations of the mutant ARs in the cytoplasm after the ligand treatment. The mutant ARs were not localized in the lysosomes, as shown by an experiment using LysoTracker, a specific marker for lysosomes (data not shown). Next, the mitochondrial localization was examined using MitoTracker, a highly specific probe for mitochondria. Many, but not all, of the cytoplasmic dots of the mutant ARs were located close to mitochondria (Fig. 8A). Because signals for the mutant ARs were not observed in the mitochondria, the mutant ARs do not seem to cross the mitochondrial membrane. To further examine the relationship between the mutant ARs and the mitochondria, immunoelectron microscopy was performed using an anti-GFP antibody. Many gold labels were present around the mitochondria, but none were found inside the mitochondria (Fig. 8Ba). Some clusters were present in the cytoplasm, and these would correspond to the cytoplasmic dots observed by the laser-scanning microscopy (Fig. 8Bb).

Discussion

Using fluorescent proteins and laser-scanning microscopy, we have demonstrated that mutations in the DBD of ARs from AIS patients impair the ligand-dependent nuclear translocation, subnuclear foci formation, and intranuclear mobility of the receptor. In our previous studies, we clearly showed that intranuclear foci formation of AR-GFP was parallel to ligand-dependent transcriptional activation of AR (5, 6). Many studies using GFP-fused steroid hormone receptors have been reported, and linkage of the foci formation of

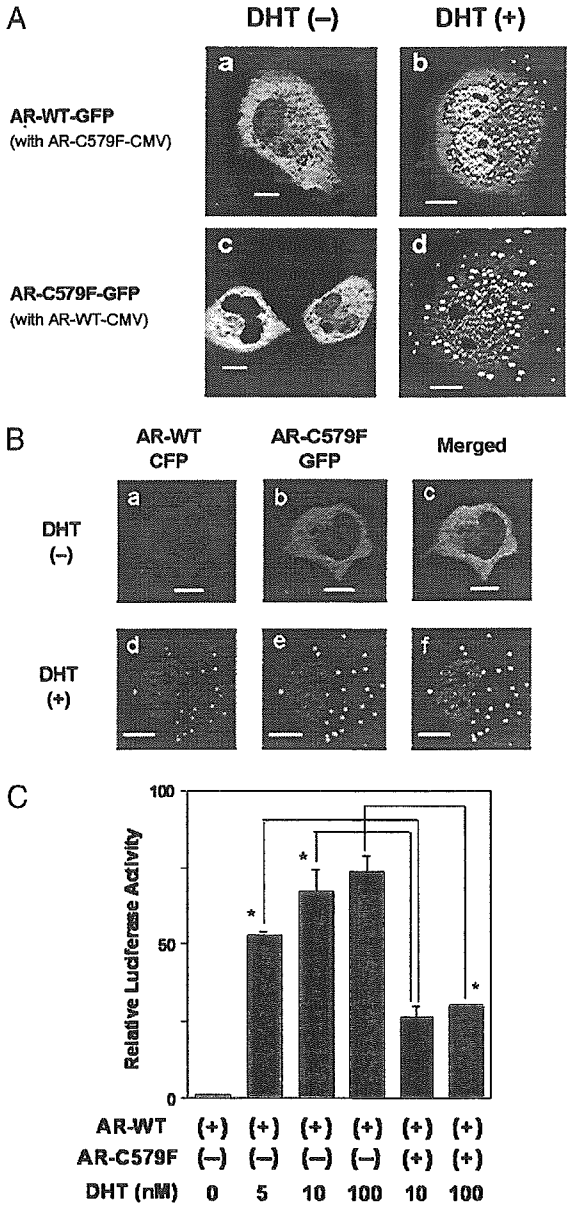

FIG. 6. Coexpression of wild-type and mutant ARs. A, a and b, Equal amounts of AR-WT-GFP and AR-C579F-CMV (without GFP) were cotransfected into COS-7 cells and images were collected before (a) and after (b) the addition of DHT. c and d, COS-7 cells expressing both AR-C579F-GFP and AR-CMV (without GFP) were observed before (c) and after (d) treatment with DHT. If AR WT and mutant proteins have equal chances to form a dimer and formed heterodimer show WT and mutant pattern of signals at an equal rate, the ratio of the intact AR signal *vs.* the abnormal one is expected to be 7:4 (b) and 4:7 (d). Signal patterns of WT and mutant in b and d were consistent with the expected ratios. *Scale bar*, 10 μm. B, Colocalization of wild-type and mutant ARs. AR-WT-CFP and AR-C579F-GFP were coexpressed in COS-7 cells in the absence or presence of DHT. Fluorescent signals were collected using the confocal microscope in the absence (a–c) or presence (d–f) of 10 nM DHT. Signals for AR-WT-CFP (d, *red*) and AR-C579F-GFP (e, *green*) were colocalized (f, merged signals). *Scale bar*, 10 μm. C, AR-C579F inhibited the transactivation mediated by the wild-type AR. COS-7 cells were cotransfected with pGL3-PSA reporter, pRL-CMV, and pAR-CMV with or without pAR-C579F-CMV. After the treatment with or without various concentrations of DHT, the cells were subjected to the luciferase assay. The *bars* show the luciferase activity relative to that of the wild-type AR without DHT. The means ± SD of three independent experiments are shown. *, $P < 0.05$.

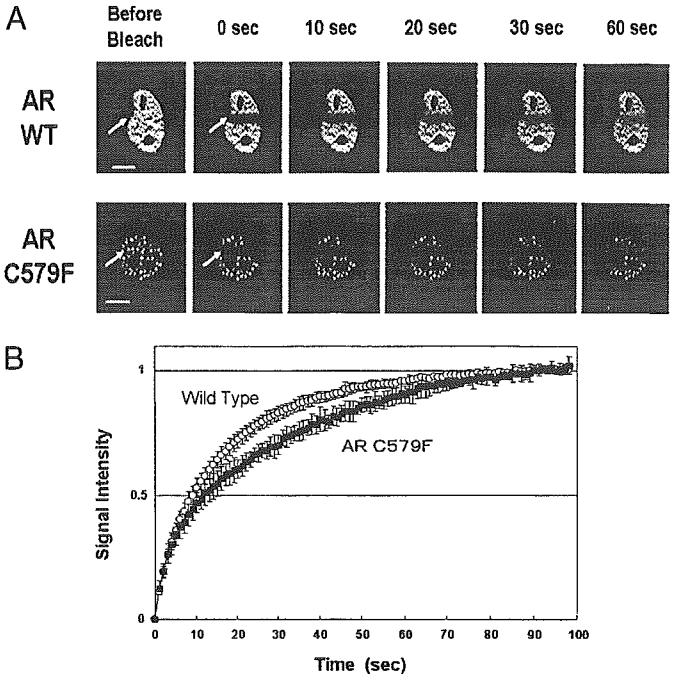

FIG. 7. Comparison of the intranuclear mobilities of the wild-type (WT) and mutant ARs by FRAP analysis. A, FRAP analysis of the intranuclear foci of the wild-type and mutant ARs. COS-7 cells were transfected with a wild-type or mutant AR expression vector. Twenty-four hours after the transfection, the cells were treated with DHT. Five hours after the addition of DHT, a region of interest in the nucleus was photobleached, and images were then taken at the indicated time points using a laser confocal microscope. *Scale bar*, 10 μm. B, Quantification of the fluorescence recovery in the FRAP analysis. The relative fluorescence intensities in the bleached areas of the wild-type and mutant AR foci were plotted. *Open circles*, intensity of the wild-type AR; *closed squares*, intensity of AR-C579F. The means ± SD of 10 cells are shown.

steroid hormone receptors with their transactivation function has been widely accepted (18–20).

There is a significant bias in the distribution of mutations of the AR gene in AIS patients, although the mutations are spread throughout the whole gene (9). Although exon 1 of the AR gene encodes more than half of the AR protein, including the transcription activation domain of the amino terminus, the number of mutations found in this exon is only about 10% of the total number of mutations, and most of the exon 1 mutations are nonsense or frameshift mutations. The mutation hot spots in AIS patients are part of the LBD constituting the pocket for androgen binding. In the DBD, 32 different mutations have been reported and 15 of these were detected in the first zinc finger motif. Most of the mutations in the DBD or LBD are single-base substitutions (3, 9). Some AIS patients do not carry any AR mutations. In such cases, there must be some abnormality in the signal transduction between the AR and the basic transcription machinery, and an impediment in a cofactor interacting with the N-terminal transcription activation domain of the AR has been suggested (14).

The amino acid substitution in the CAIS patient (subject 1) occurred at the cysteine residue contained in the first zinc finger motif of the AR. This AR-C579F mutant would not be able to coordinate the zinc ion, resulting in complete loss of the ligand-dependent DNA-binding ability. In the PAIS patient,

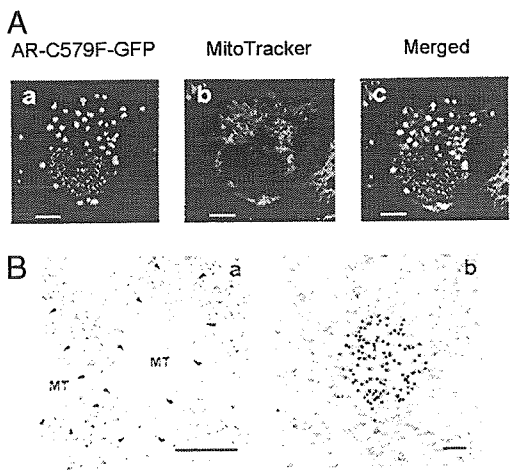

FIG. 8. Mitochondrial localization of cytoplasmic AR-C579F. A, COS-7 cells were transfected with 0.5 μg of AR-C579F-GFP. Twenty-four hours after the transfection, the cells were treated with 10^{-8} M DHT. After a 1-h incubation with DHT, 200 nM MitoTracker-Orange was added to the medium, and the cells were incubated for 30 min. After washing with PBS, the cells were observed under a laser confocal microscope. *Green signals*, AR-C579F-GFP; *red signals*, mitochondria. *Scale bar*, 10 μm. B, Immunoelectron microscopy of the AR-C579F mutant. After treatment with DHT, COS-7 cells expressing AR-C579F-GFP were fixed, embedded, and incubated with an anti-GFP antibody at 4 C overnight, followed by incubation with colloidal gold-conjugated goat antirabbit IgG. Sections were stained and observed with an electron microscope as described in *Subjects and Methods*. a, Low resolution (*bar*, 1 μm); b, high resolution (*bar*, 0.1 μm). MT, Mitochondria. The *arrowheads* show the edges of the mitochondria.

the amino acid substitution (F582Y) occurred next to the P-box and may cause a conformational change of the zinc finger motif. The impaired DNA-binding of these mutant ARs was confirmed by gel mobility shift assays, as we previously reported (11). Before the present imaging analysis, it was anticipated that these mutants would be able to enter the nucleus after ligand treatment but be unable to form foci like the wild-type AR due to the loss of the DNA-binding capacity. However, these mutant ARs initially formed cytoplasmic dots instead of the nuclear foci and nuclear dots subsequently appeared. Because there were no differences among the localizations of the wild-type and mutant ARs in the absence of the ligand, the conformations of the ligand-bound mutant ARs are considered to differ from that of the wild-type AR.

In the present study, ligand-induced formation of cytoplasmic dots of the mutant ARs was observed close to the mitochondria. However, the mutant AR signals were not detected inside the mitochondria by immunoelectron microscopy. Similar findings of an association between cytoplasmic protein aggregates and mitochondria have been observed for other mutant proteins, including the polyQ AR mutants (21–24). The mechanism for such aggregation close to mitochondria has been speculated to be that the ubiquitin-proteasome system tries to degrade a large amount of aggregated proteins and therefore requires an increased amount of ATP around the protein inclusions. The mechanism of localization close to mitochondria for the polyQ AR mutant might also occur for our AR-DBD mutants, although pathophysiology is quite different between our AIS and polyQ diseases. However, further study is necessary for elucidation of abnormal dot formation of our AR mutants.

The C579F mutation in the AR-DBD showed lower mobility than the wild-type AR. FRAP analysis has recently been used to examine the intranuclear dynamics of nuclear receptors (25–27). In the presence of ligands, the mobility of the nuclear receptors was reduced. It has been reported that ligand-induced intranuclear foci formation of steroid hormone receptors is associated with the nuclear matrix in which coactivators are also recruited (28). This nuclear matrix binding induced by ligand treatment is suggested to cause the decreased mobility of the receptors. A glucocorticoid receptor (GR) mutant carrying a deletion of the N-terminal region showed a much lower mobility (26). This mutant was deprived of all the putative phosphorylation sites of the GR. In ATP-deprived cells, GRs are dephosphorylated and tightly bound to the nuclear matrix (29, 30). Therefore, it has been speculated that appropriate reduction of the mobility of steroid hormone receptors, namely nuclear matrix binding with coactivators (6, 31–33), is an essential process for the normal transactivation functions of steroid hormone receptors. Lower or much increased mobility of ligand-bound steroid hormone receptors, as shown for the present AR C579F mutant, may indicate an impaired transactivation process.

The present reanalysis of our mutant ARs unexpectedly revealed two kinds of functional defects, *i.e.* lack of DNA-binding ability reported previously (11) and impairment of translocation from the cytoplasm to the nucleus. The finding that mutations in DNA-binding domain of AR impair nuclear translocation is novel and suggests the existence of an important intramolecular domain for nuclear translocation except for the hinge region. This finding is expected to contribute to the study of translocation mechanism. A mutant AR, K632A/K633A, which has mutations in the hinge region, has an intact DNA-binding domain, but its nuclear translocation is impaired (34). The pattern of the translocation impairment of this AR-K632A/K633A mutant was quite similar to that of our AR mutants, namely the AR-K632A/K633A mutant formed cytoplasmic aggregates (large dots) and its transactivation function examined by a reporter luciferase assay was markedly low (34, 35).

These reported results clearly indicate that impairment of nuclear translocation such as cytoplasmic dot formation can be responsible for the suppression of transactivation function of AR. As is well known, for transactivation function of AR, AR first must be translocated into the nucleus, secondly form a complex with coactivators, and then bind to target genes. Therefore, it would be reasonable that impairment of nuclear translocation in AR-C579F and AR-F582Y is largely responsible for AIS. Abnormal dot formation and decreased mobility of liganded AR-DBD mutants in the nucleus might be due to lack of DNA-binding ability, and thus, a defect in DNA-binding also would be responsible for AIS to some extent. Recent studies have revealed dynamic movement of nuclear receptors during a transactivation process within the nucleus (25, 36, 37). Liganded steroid hormone receptors including AR are transferred to subnuclear compartments (foci) and form a complex with coactivators. These receptor-coactivator complexes are mobilized to the target genes. The

steroid hormone receptors and coactivators show multiphasic on and off for binding to promoter elements of genes. The receptor-coactivator complexes also undergo a rapid exchange between target genes and the compartments. The present AR-DBD mutants are not able to access target genes. This may disturb the dynamic movement (mobility), resulting in prolonged stay at nuclear matrix and abnormal dot formation. This speculation may be supported by the reported observation that the AR-K632A/K633A mutant did not show abnormal intranuclear dot formation, although the authors did not touch on it.

In conclusion, the AR-DBD mutations, C579F and F582Y, found in our AIS patients showed abnormalities in ligand-dependent nuclear translocation, nuclear matrix targeting, and intranuclear mobility of the receptor, which may cause AIS in these patients.

Acknowledgments

We thank Mitoshi Toki for his excellent technical assistance in performing the three-dimensional imaging analyses.

Received January 27, 2005. Accepted August 15, 2005.

Address all correspondence and requests for reprints to: Ryoichi Takayanagi, Department of Geriatric Medicine, Graduate School of Medical Sciences, Kyushu University, 3-1-1 Maidashi, Higashi-ku, Fukuoka 812-8582, Japan. E-mail: takayana@geriat.med.kyushu-u.ac.jp.

This work was supported in part by grants-in-aid for Scientific Research and Exploratory Research and a grant for the 21st Century Center of Excellence Program (Kyushu University) from the Japanese Ministry of Education, Culture, Sports, Science, and Technology.

References

1. **Gobinet J, Poujol N, Sultan Ch** 2002 Molecular action of androgens. Mol Cell Endocrinol 198:15–24
2. **Aranda A, Pascual A** 2001 Nuclear hormone receptors and gene expression. Physiol Rev 81:1269–1304
3. **Brinkmann AO** 2001 Molecular basis of androgen insensitivity. Mol Cell Endocrinol 179:105–109
4. **Roy AK, Tyagi RK, Song CS, Lavrovsky Y, Ahn SC, Oh TS, Chatterjee B** 2001 Androgen receptor: structural domains and functional dynamics after ligand-receptor interaction. Ann NY Acad Sci 949:44–57
5. **Tomura A, Goto K, Morinaga H, Nomura M, Okabe T, Yanase T, Takayanagi R, Nawata H** 2001 The subnuclear three-dimensional image analysis of androgen receptor fused to green fluorescence protein. J Biol Chem 276:28395–28401
6. **Saitoh M, Takayanagi R, Goto K, Fukamizu A, Tomura A, Yanase T, Nawata H** 2002 The presence of both the amino- and carboxyl-terminal domains in the AR is essential for the completion of a transcriptionally active form with coactivators and intranuclear compartmentalization common to the steroid hormone receptors: a three-dimensional imaging study. Mol Endocrinol 16:694–706
7. **Gelmann EP** 2002 Molecular biology of the androgen receptor. J Clin Oncol 20:3001–3015
8. **Balducci R, Ghirri P, Brown TR, Bradford S, Boldrini A, Boscherini B, Sciarra F, Toscano V** 1996 A clinician looks at androgen resistance. Steroids 61:205–211
9. **Gottlieb B, Pinsky L, Beitel LK, Trifiro M** 1999 Androgen insensitivity. Am J Med Genet 89:210–217
10. **McPhaul MJ** 2002 Androgen receptor mutations and androgen insensitivity. Mol Cell Endocrinol 198:61–67
11. **Imasaki K, Okabe T, Murakami H, Tanaka Y, Haji M, Takayanagi R, Nawata H** 1996 Androgen insensitivity syndrome due to new mutations in the DNA-binding domain of the androgen receptor. Mol Cell Endocrinol 120:15–24
12. **Ishizuka M, Kawate H, Takayanagi R, Ohshima H, Tao RH, Hagiwara H** 2005 A zinc finger protein TZF is a novel corepressor of androgen receptor. Biochem Biophys Res Commun 331:1025–1031
13. **Nakao R, Haji M, Yanase T, Ogo A, Takayanagi R, Katsube T, Fukumaki Y, Nawata H** 1992 A single amino acid substitution (Met786–Val) in the steroid-binding domain of human androgen receptor leads to complete androgen insensitivity syndrome. J Clin Endocrinol Metab 74:1152–1157
14. **Adachi M, Takayanagi R, Tomura A, Imasaki K, Kato S, Goto K, Yanase T, Ikuyama S, Nawata H** 2000 Androgen-insensitivity syndrome as a possible coactivator disease. N Engl J Med 343:856–862
15. **Kawate H, Wu Y, Ohnaka K, Nawata H, Takayanagi R** 2005 Tob proteins suppress steroid hormone receptor-mediated transcriptional activation. Mol Cell Endocrinol 230:77–86
16. **Luby-Phelps K, Ning G, Fogerty J, Besharse JC** 2003 Visualization of identified GFP-expressing cells by light and electron microscopy. J Histochem Cytochem 51:271–274
17. **Ham J, Thomson A, Needham M, Webb P, Parker M** 1988 Characterization of response elements for androgens, glucocorticoids and progestins in mouse mammary tumour virus. Nucleic Acids Res 16:5263–5276
18. **Kawata M** 2001 Subcellular steroid/nuclear receptor dynamics. Arch Histol Cytol 64:353–368
19. **DeFranco DB** 2002 Navigating steroid hormone receptors through the nuclear compartment. Mol Endocrinol 16:1449–1455
20. **Hager GL, Nagaich AK, Johnson TA, Walker DA, John S** 2004 Dynamics of nuclear receptor movement and transcription. Biochim Biophys Acta 1677:46–51
21. **Stenoien DL, Cummings CJ, Adams HP, Mancini MG, Patel K, DeMartino GN, Marcelli M, Weigel NL, Mancini MA** 1999 Polyglutamine-expanded androgen receptors from aggregates that sequester heat shock proteins, proteasome components and SRC-1, and are suppressed by the HDJ-2 chaperone. Hum Mol Genet 8:731–741
22. **Waelter S, Boeddrich A, Lurz R, Scherzinger E, Lueder G, Lehrach H, Wanker EE** 2001 Accumulation of mutant huntingtin fragments in aggresome-like inclusion bodies as a result of insufficient protein degradation. Mol Biol Cell 12:1393–1407
23. **Milewski MI, Mickle JE, Forrest JK, Stanton BA, Cutting GR** 2002 Aggregation of misfolded proteins can be a selective process dependent upon peptide composition. J Biol Chem 277:34462–34470
24. **Piccioni F, Pinton P, Simeoni S, Pozzi P, Fascio U, Vismara G, Martini L, Rizzuto R, Poletti A** 2002 Androgen receptor with elongated polyglutamine tract forms aggregates that alter axonal trafficking and mitochondrial distribution in motoneuronal processes. FASEB J 16:1418–1420
25. **Stenoien DL, Patel K, Mancini MG, Dutertre M, Smith CL, O'Malley BW, Mancini MA** 2001 FRAP reveals that mobility of oestrogen receptor-α is ligand- and proteasome-dependent. Nat Cell Biol 3:15–23
26. **Schaaf MJ, Cidlowski JA** 2003 Molecular determinants of glucocorticoid receptor mobility in living cells: the importance of ligand affinity. Mol Cell Biol 23:1922–1934
27. **Maruvada P, Baumann CT, Hager GL, Yen PM** 2003 Dynamic shuttling and intranuclear mobility of nuclear hormone receptors. J Biol Chem 278:12425–12432
28. **Stenoien DL, Mancini MG, Patel K, Allegretto EA, Smith CL, Mancini MA** 2000 Subnuclear trafficking of estrogen receptor-α and steroid receptor coactivator-1. Mol Endocrinol 14:518–534
29. **Hu LM, Bodwell J, Hu JM, Orti E, Munck A** 1994 Glucocorticoid receptors in ATP-depleted cells. Dephosphorylation, loss of hormone binding, HSP90 dissociation, and ATP-dependent cycling. J Biol Chem 269:6571–6577
30. **Tang Y, DeFranco DB** 1996 ATP-dependent release of glucocorticoid receptors from the nuclear matrix. Mol Cell Biol 16:1989–2001
31. **Georget V, Térouanne B, Lumbroso S, Nicolas J-C, Sultan C** 1998 Trafficking of androgen receptor mutants fused to green fluorescent protein: a new investigation of partial androgen insensitivity syndrome. J Clin Endocrinol Metab 83:3597–3603
32. **Nazareth LV, Stenoien DL, Bingman III WE, James AJ, Wu C, Zhang Y, Edwards DP, Mancini M, Marcelli M, Lamb DJ, Weigel NL** 1999 A C619Y mutation in the human androgen receptor causes inactivation and mislocalization of the receptor with concomitant sequestration of SRC-1 (steroid receptor coactivator 1). Mol Endocrinol 13:2065–2075
33. **Karvonen U, Janne OA, Palvimo JJ** 2002 Pure antiandrogens disrupt the recruitment of coactivator GRIP1 to colocalize with androgen receptor in nuclei. FEBS Lett 523:43–47
34. **Thomas M, Dadgar N, Aphale A, Harrell JM, Kunkel R, Pratt WB, Lieberman AP** 2004 Androgen receptor acetylation site mutations cause trafficking defects, misfolding, and aggregation similar to expanded glutamine tracts. J Biol Chem 279:8389–8395
35. **Fu M, Wang C, Reutens AT, Wang J, Angeletti RH, Siconolfi-Baez L, Ogryzko V, Avantaggiati ML, Pestell RG** 2000 p300 and p300/cAMP-response element-binding protein-associated factor acetylate the androgen receptor at sites governing hormone-dependent transactivation. J Biol Chem 275:20853–20860
36. **Métivier R, Penot G, Hübner MR, Reid G, Brand H, Koš M, Gannon F** 2003 Estrogen receptor-α directs ordered, cyclical, and combinational recruitment of cofactors on a natural target promoter. Cell 115:751–763
37. **McNally JG, Muller WG, Walker D, Wolford R, Hager GL** 2000 The glucocorticoid receptor: rapid exchange with regulatory sites in living cells. Science 287:1262–1265

JCEM is published monthly by The Endocrine Society (http://www.endo-society.org), the foremost professional society serving the endocrine community.

ELSEVIER

Molecular and Cellular Endocrinology 230 (2005) 77–86

MCE
Molecular and Cellular Endocrinology
www.elsevier.com/locate/mce

Tob proteins suppress steroid hormone receptor-mediated transcriptional activation

Hisaya Kawate[a], Yin Wu[a], Keizo Ohnaka[a], Hajime Nawata[b], Ryoichi Takayanagi[a,*]

[a] *Department of Geriatric Medicine, Graduate School of Medical Sciences, Kyushu University, 3-1-1 Maidashi, Higashi-ku, Fukuoka 812-8582, Japan*
[b] *Department of Medicine and Bioregulatory Science, Graduate School of Medical Sciences, Kyushu University, 3-1-1 Maidashi, Higashi-ku, Fukuoka 812-8582, Japan*

Received 17 May 2004; received in revised form 10 October 2004; accepted 21 October 2004

Abstract

Although sex steroid hormones have significant effects on bone metabolism, the molecular mechanisms of these actions have not been fully elucidated yet. We examined the functional relationship between steroid hormone receptors and Tob, a member of an anti-prolifelative protein family and a negative regulator of osteoblast proliferation and differentiation. Luciferase assay using promoters carrying hormone-responsive elements revealed that both Tob1 and Tob2 proteins but not PC3 suppressed steroid hormone receptor-dependent transcriptional activation in MC3T3-E1 osteoblastic cells. Mutated Tob proteins carrying amino acid substitutions at an LXXLL motif also showed the same degree of inhibition of the transcriptional activation as the wild type. By observation of androgen receptor (AR)-tagged with green fluorescent protein under a confocal laser scanning microscope, we found that Tob1 inhibits the nuclear foci formation of dihydrotestosterone-bound AR. These results indicate that Tob family proteins may negatively regulate sex steroid hormone action in bone formation.
© 2004 Elsevier Ireland Ltd. All rights reserved.

Keywords: Steroid hormone receptor; Osteoblast; GFP; LXXLL motif; Androgen

1. Introduction

Sex steroid hormones play important roles not only in the reproductive system but also in bone metabolism. It is well known that estrogen deficiency after menopause is the most important factor in osteoporosis development among women. Estrogen replacement is one of the major therapies for female postmenoposal osteoporosis. On the other hand, loss of androgen function also causes various abnormalities in bone metabolism (Hofbauer and Khosla, 1999; Manolagas et al., 2002). As well as ovariectomy, orchidectomized mice exhibited marked bone loss due to excessive bone resorption (Onoe et al., 2000). More recently, androgen receptor-deficient mice were generated and showed decreased bone volume with increased bone resorption (Yeh et al., 2002; Kawano et al., 2003).

In the last few years, the mechanism of steroid hormone action in a cell has been extensively studied at molecular level. After steroid hormones enter their target cells, these hormones bind to their specific receptors. Ligand-bound receptors change their conformation and regulate transcription by binding to hormone responsive elements located in regulatory regions of target genes. The effects of nuclear receptors on transcription are modulated by coregulator proteins, which enhance (coactivators) or reduce (corepressors) transactivation of target genes. Many of these coactivators possess histone acetylase activity, whereas corepressor complexes often contain histone deacetylase activity. Reversible acetylation of core histones modulates chromatin structure and regulates transcription. These coactivators commonly possess an LXXLL motif in their amino acid sequences through which they can interact with steroid hormone receptors. Introducing mutations in this motif abolished the function of these coactivators (Leo and Chen, 2000; Aranda and Pascual, 2001; Cheng et al., 2002; Heinlein and Chang, 2002).

* Corresponding author. Tel.: +81 92 6426913; fax: +81 92 6426940.
E-mail address: takayana@geriat.med.kyushu-u.ac.jp (R. Takayanagi).

0303-7207/$ – see front matter © 2004 Elsevier Ireland Ltd. All rights reserved.
doi:10.1016/j.mce.2004.10.009

Tob, which was originally discovered as a protein interacting with a membrane receptor c-erbB2, is a member of a functionally and structurally related protein family involved in negative control of the cell cycle (Matsuda et al., 1996; Ikematsu et al., 1999; Matsuda et al., 2001; Tirone, 2001). This family comprises six proteins; Tob1, Tob2, BTG1, BTG2/PC3/TIS21, ANA/BTG3 and PC3B. These proteins share a homology at N-terminal 120 amino acid residues. Anti-proliferating activity of Tob protein is regulated by phosphorylation of three serine residues (Ser152, 154 and 164) that are modified by Erk MAP Kinase. In quiescent cells, Tob1 blocks their proliferation by suppression of cyclin D1 expression. Growth signals activate Erk that phosphorylates Tob protein to lose its anti-proliferating activity, resulting in continuous expression of cyclin D1 and cell cycle progression (Maekawa et al., 2002; Suzuki et al., 2002; Yoshida et al., 2003).

It has been indicated that Tob member proteins would mainly act on transcription. These proteins have been shown to physically interact with Caf1, whose yeast homologue is involved in a transcription complex (Rouault et al., 1998; Ikematsu et al., 1999; Prevot et al., 2001). Furthermore, four of the Tob family proteins carry an LXXLL motif being common in coactivators for nuclear receptors. In fact, BTG1 and BTG2 modulate the estrogen receptor (ER)-mediated transcriptional activation through this LXXLL motif (Prevot et al., 2001).

Mice carrying a targeted deletion of the *Tob* gene have a greater bone mass resulting from increased numbers of osteoblasts. Bone morphogenetic protein-2 (BMP-2), a member of the transforming growth factor-beta (TGF-β) superfamily, has been shown to control osteoblast proliferation and differentiation. BMP signals are mainly mediated by Smad proteins. In these Tob-deficient mice, BMP-2-induced osteoblast proliferation and differentiation was enhanced. Tob was shown to associate with receptor-regulated Smads (Smad1, 5 and 8), which are the mediators of BMP signals, and inhibit the signal transduction. These results indicate that Tob protein negatively regulates bone formation in vivo by repressing BMP-2-induced, Smad-mediated transcriptional activation (Yoshida et al., 2000).

In the present study, we investigated whether Tob expression influences steroid hormone receptor-dependent transcriptional activation in osteoblasts. Tob proteins suppressed the ligand-dependent transcriptional activation of steroid hormone receptors such as androgen receptor (AR) and estrogen receptor (ER) in osteoblastic cells. These results indicate that Tob proteins could regulate the action of steroid hormone in bone formation.

2. Materials and methods

2.1. Cells

MC3T3-E1 osteoblastic cells were obtained from Riken Cell Bank (Tokyo, Japan). Cells were maintained in α-MEM (Invitrogen Corp., Carlsbad, CA) supplemented with 10% fetal bovine serum (FBS) (Cansera International Inc., Canada). COS-7 monkey kidney cells were maintained in DMEM (Invitrogen) with 10% FBS and PC3 prostatic carcinoma cells were maintained in RPMI-160 medium (Sigma-Aldrich Co., St. Louis, MO).

2.2. Plasmid constructs

The firefly luciferase reporter plasmid, pGL3-MMTV (Tomura et al., 2001) and the expression vector for AR (pCMV-hAR) were prepared as previously described (Nakao et al., 1992; Adachi et al., 2000). The expression plasmid for human ERα (pSG5-ERα) and a reporter plasmid (pERE2-tk109-luc) were kindly provided by Dr. Shigeaki Kato (University of Tokyo, Japan). Plasmid vector expressing AR-GFP fusion protein, named pAR-GFP, was constructed as described previously (Tomura et al., 2001). A 644-bp fragment of 5′-flanking region of the prostate specific antigen (PSA) gene was amplified by KOD DNA polymerase (Toyobo, Osaka, Japan) using a set of primers: PSAP-N (5′-aggtaccgaattccacattgtttgctgc-3′) and PSAP-C (5′-tccgggtgcaggtggtaagcttgg-3′). The PCR-amplified fragment was digested with *Kpn*I and *Hind*III and cloned into pGL3-Basic vector (Promega Co., Madison, WI) and the resulting construct was named pGL3-PSA. Mouse CREB binding protein (CBP) expression vector (pcDNA/mCBP) was prepared as previously described (Miyagishi et al., 2000). TIF2 expression plasmid, pYFP-TIF2, was constructed as previously described (Saitoh et al., 2002).

The expression vectors for Tob proteins were prepared using the RT-PCR technique. As previously described (Ohnaka et al., 2001), cDNA was prepared from human osteoblasts using Superscript First-Strand Synthesis System (Invitrogen). Tob1, Tob2 and PC3 cDNAs were amplified by Pfx DNA polymerase (Invitrogen) using each set of primers: Tob1-5E (5′-caggaattcggggagttgaaaccta-3′) and Tob1-3B (5′-cagggatcccggttagccataacagg-3′) for Tob1, Tob2-5E (5′-caggaattccaaggctgtacacgtgc-3′) and Tob2-3B (5′-cagggatcccggttggccagcaccacg-3′) for Tob2, and PC3-5E (5′-caggaattccacccgagacctctca-3′) and PC3-3B (5′-cagggatcccggctggagactgccatc-3′) for PC3. The PCR-amplified fragments were digested with *Eco*RI and *Bam*HI and inserted into the cognate sites of pEYFP-C1 vector (BD Sciences Clontech, Palo Alto, CA). The resulting constructs were designated as pYFP-Tob1, pYFP-Tob2 and pYFP-PC3. To generate Tob1 LXXAA mutant, two leucine residues in the LXXLL motif of the Tob protein were replaced with alanines by using a Quikchange site-directed mutagenesis kit (Stratagene, La Jolla, CA). The validity of structure of the constructs was confirmed by DNA sequencing using an ABI PRISM 377 DNA sequencer (Applied Biosystems Japan Ltd., Tokyo, Japan).

2.3. Immunoblotting

MC3T3-E1 cells were seeded in 60-mm plates and incubated for 24 h with 5% CO_2 at 37 °C. Plasmid DNAs carrying Tob family cDNAs were transfected into the cells. Twenty-four hours after transfection, cells were washed with PBS twice and 400 μl of NP-40 lysis buffer (50 mM Tris–HCl, pH 8.0, 150 mM NaCl and 1% NP-40) was added to each dish, followed by rocking for 30 min at 4 °C. Lysates were collected and protein concentrations were measured using a BCA protein assay kit (Pierce, Rockford, IL). Forty micrograms of each lysate in 1× sodium dodecyl sulfate (SDS)-PAGE sample buffer (2% SDS, 100 mM dithiothreitol, 60 mM Tris–HCl, pH 6.8, 0.01% bromophenol blue) was loaded on a 10% SDS-polyacrylamide gel with wide range Color Marker (Sigma-Aldrich) and electrophoresis was performed at 20 mA for 4 h. Proteins were transferred onto a nitrocellulose membrane (Hybond ECL, Amersham Bioscience Corp., Piscataway, NJ) using a Hoefer miniVe unit (Amersham) at 250 V for 1 h at 25 °C. After the membrane was blocked in 1× Block-Ace (Dainippon Pharmaceutical Co., Osaka, Japan), anti-Tob1 mouse monoclonal antibody (IBL-Japan, Fujioka, Japan) or anti-GFP rabbit polyclonal antibody (sc-8334, Santa Cruz Biotechnology Inc., Santa Cruz, CL) was reacted with the membrane in 0.1× Block-Ace for 1 h at 25 °C. Following a brief wash with TBS–Tween 20 (10 mM Tris–HCl, pH 8.0, 0.9% NaCl and 0.05% Tween 20), horseradish peroxidase-linked anti-mouse IgG (Amersham) or anti-rabbit IgG (Amersham) was added in 0.1× Block-Ace as a second antibody and then the membrane was incubated for 45 min at 25 °C. After being washed with TBS–Tween 20, the membrane was reacted with Western blotting detection reagents (Amersham) for 1 min in a dark room. The membrane was then exposed to a sheet of autoradiography film for 1 min and the film was developed and analyzed.

2.4. Functional reporter assay

MC3T3-E1 cells (7×10^4 cells/well), COS-7 cells (1×10^5 cells/well) or PC3 cells (1×10^5 cells/well) were seeded in 12-well plates 20 h before transfection. A reporter plasmid, pGL3-MMTV or pGL3-PSA (0.5 μg/well), and 3 ng/well of pRL-CMV (Promega) as an internal control were cotransfected with 0.1 μg/well of pCMV-hAR and 0.1 or 0.3 μg of the Tob expression plasmid using 2.7 μl/well of Superfect Transfection Reagent (Qiagen K. K., Tokyo, Japan). For ER transcription assay, 0.1 μg/well of pSG5-ERα and 0.1 or 0.3 μg of the Tob expression vector were cotransfected with 0.5 μg of pERE2-tk109-luc as a reporter and 3 ng of pRL-CMV as an internal control. For CBP or TIF2 transfection, 0.1 or 0.3 μg of pcDNA/mCBP or 0.5 μg of pYFP-TIF2 was used for each well. In all transfection experiments, the total amount of transfected DNA was fixed by adding empty vector into the transfection mixture. At 3 h post-transfection, 0.5 ml of medium containing 10% charcoal-treated fetal bovine serum was added with or without steroid hormones. At 24 h post-transfection, cells were rinsed with PBS and lysed in the lysis buffer of a luciferase assay kit (Promega). The luciferase activity was assayed using a Dual-Luciferase Assay System (Promega Corp., Madison, WI) and Lumat LB 9507 (Berthold Technologies, Bad Wildbad, Germany). Data were presented as mean ± S.D. One-way analysis of variance followed by Scheffe's test was used for multigroup comparisons. $P < 0.05$ was considered to be statistically significant.

2.5. Coimmunoprecipitation

COS-7 cells (7×10^5 cells/dish) were seeded in 60-mm plates 24 h before transfection. Cells were transfected with 2 μg of plasmids expressing Tob and/or AR and maintained with or without 10^{-8} M of DHT for 24 h with 5% CO_2 at 37 °C. The whole cell extracts were prepared by incubating the cells in 0.3 ml of the NP-40 lysis buffer for 30 min at 4 °C, followed by brief sonication and a centrifugation. Protein concentrations were measured using a BCA protein assay kit (Pierce) and each protein concentration was adjusted to 1 mg/ml. Each lysate (160 μg) was incubated with 3 μg of anti-Tob antibody (IBL-Japan) at 4 °C for 1 h in the NP-40 lysis buffer and further incubated with 25 μl of Protein G Magnetic Beads (New England Biolabs Inc., Beverly, MA) for 1 h at 4 °C. Beads were collected by a magnet and then proteins were eluted in 1× SDS-PAGE sample buffer and subjected to 10% SDS-PAGE. Immunoblotting analysis was performed essentially as previously described (Ohnaka et al., 2001).

2.6. Confocal laser scanning microscopy

MC3T3-E1 cells (2×10^5 cells/dish) were cultured in 35-mm glass-bottom dishes (Asahi Techno Glass Corp., Tokyo, Japan) and transfected with 0.5 μg of pAR-GFP and 1.5–2.5 μg of pYFP-Tob1 using 10 μl/well of Superfect Transfection Reagent. The cells were maintained in α-MEM supplemented with 10% charcoal-treated FBS for 16–20 h and then various steroid hormones were added into the medium.

The cells were observed with an LSM 510 META invert confocal laser scanning microscope (Carl Zeiss Co. Ltd., Jena, Germany) using a 100×, 1.4 numerical aperture oil immersion objective. Images were collected at a 12-bit depth resolution of intensities over 1024 × 1024 pixels. For excitation of GFP and YFP, 488 nm of argon laser was employed and these two emission signals were separated using the emission fingerprinting technique established by Carl Zeiss. Separation of individual emission signals was based on recording of a spectral signature of each emission signal and a digital unmixing procedure using the reference spectra.

3. Results

3.1. Suppression of steroid hormone receptor-mediated transcriptional activation by Tob protein

We investigated whether Tob family proteins modulate the function of steroid hormone receptors in osteoblasts because some of Tob family proteins have one or two copies of an LXXLL motif that is commonly found in interaction domains of coactivators for nuclear receptors (Fig. 1). To examine whether expression of the Tob family proteins influences the transcriptional activation mediated by steroid hormone receptors, cotransfection of AR and Tob expression plasmids was performed with the MMTV-luciferase reporter gene into MC3T3-E1 osteoblastic cells. Expression of Tob family proteins in the transfected cells was confirmed by immunoblotting using anti-Tob1 and anti-GFP antibodies (Fig. 2A). We first examined an effect of Tob1 expression on transactivation mediated by endogenous AR protein, however, ligand-induced increase of luciferase activity was not evident and no significant change of the transactivation was observed by expressing the Tob protein (Fig. 2B). In the wild type AR-transfected cells, remarkable transcriptional activation was observed in the presence of dihydrotestosterone (DHT). Tob1 and Tob2 proteins suppressed this DHT-induced transcriptional activation mediated by AR in MC3T3-E1 cells, whereas expression of PC3 had no effect on the transcriptional activation in spite of carrying two LXXLL motifs (Fig. 2B). As well as AR, transcriptional activation mediated by ERα was also repressed by Tob proteins (Fig. 2C). These Tob1-induced repressions for the steroid hormone receptor-mediated transactivation were also observed in case of different cells (PC3 and COS-7 cells) and a different promoter (PSA promoter) (Fig. 3).

3.2. An LXXLL motif of Tob1 protein is not critical for suppression of AR-mediated transactivation

To investigate whether the suppression of transcriptional activation was elicited through an LXXLL motif in the Tob1 protein, we constructed a Tob1 mutant carrying amino acid substitutions in this motif (LXXAA). As shown in Fig. 4, this Tob1 LXXAA mutant caused the same level of suppression of AR-mediated transactivation as the wild type. This result indicates that the LXXLL motif in the Tob1 protein is not crucial to the suppression of the AR-mediated transactivation. We also found an LXXII motif in the N-terminus of the Tob1 protein, which was known as an interaction domain of some nuclear receptor corepressors (Hu and Lazar, 1999). However, no significant effects were observed by introduction of mutations (LXXAA) at the LXXII motif (data not shown).

3.3. Suppression of the AR-mediated transactivation by Tob was not recovered by overexpression of CBP and TIF2

Several transcriptional coactivators were shown to be commonly involved in various transcriptional factor complexes, and the presence of a competition between these transcription complexes for limited amounts of the coactivators in a cell has been reported (Kamei et al., 1996). CBP/p300 is known to be such a common coactivator. If the Tob protein would extract CBP/p300 from the AR-mediated transactivation function complex, supplementation of the CBP protein might recover from the suppression by the Tob protein. To examine this possibility, CBP was coexpressed with Tob and AR in MC3T3-E1 cells. As shown in Fig. 5A, CBP promoted the AR-mediated transactivation dose-dependently. However, overexpression of the CBP protein had little effect on suppression of AR-mediated transcriptional activation by Tob. We also supplemented another common coactivator protein, TIF2, and no recovery from the suppression was observed (Fig. 5B).

3.4. Immunoprecipitation of Tob protein with AR

To test for a physical interaction between Tob1 and AR, immunoprecipitation was performed using anti-Tob1 antibody. In the cells expressing both AR and Tob1, AR protein

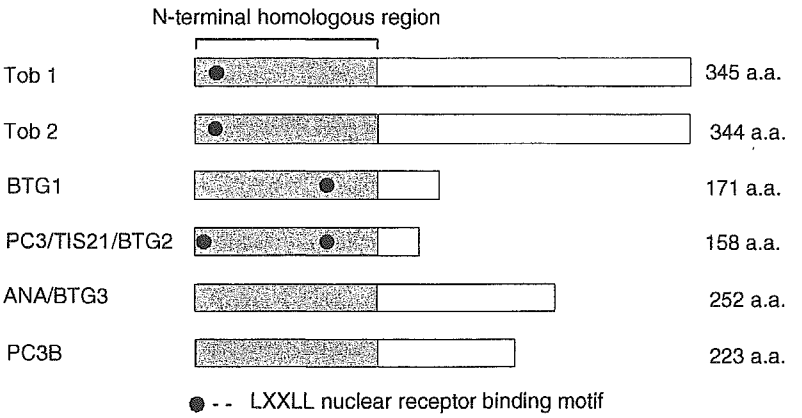

Fig. 1. Schematic representation of Tob family proteins. Six Tob family proteins share homology at the N-terminal region (gray). Filled circles represent LXXLL motifs that are noticed as interaction domains of nuclear receptor coregulators.

was clearly precipitated in the presence and absence of a ligand (Fig. 6, lanes 1–2). However, if Tob protein was not introduced into the cells, only a faint AR band was detected (Fig. 6, lane 3). The small amount of AR might be precipitated with endogenous Tob protein. These results indicate the direct interaction between Tob1 and AR and suggest that a protein-protein interaction between Tob and AR contributes to the repression of AR-mediated transcriptional activation.

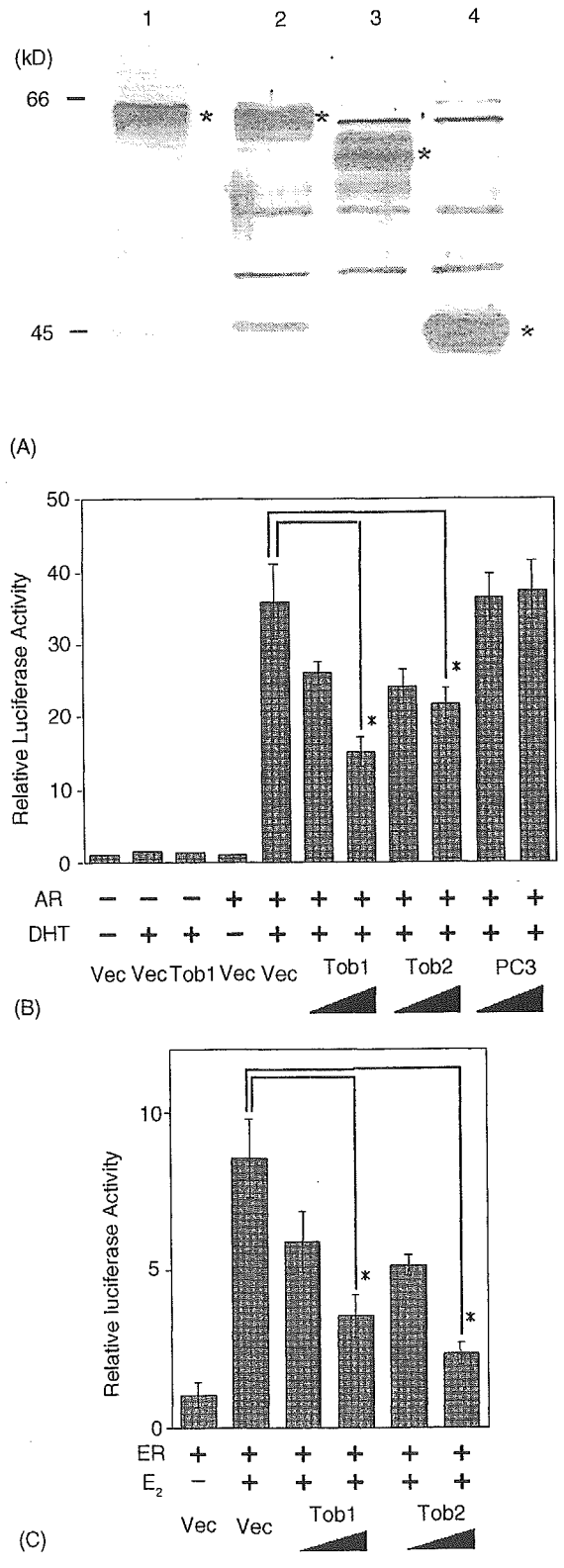

3.5. Effect of Tob1 expression on formation of subnuclear AR foci

We previously reported that ligand-bound AR was translocated from cytoplasm to nucleus and formed subnuclear foci. This foci formation of AR correlated with AR-mediated transcriptional activation (Tomura et al., 2001; Saitoh et al., 2002). To examine the effect of Tob on the AR foci formation, we observed intracellular localization of the Tob protein. In MC3T3-E1 cells, Tob1 and Tob2 proteins were localized in both nucleus and cytoplasm. Signal strength of Tob1 in the nucleus is higher than that in the cytoplasm, whereas the cytoplasmic signal is dominant in terms of Tob2 (Fig. 7). When the YFP vector, carrying only a YFP cDNA, and pAR-GFP were transfected into MC3T3-E1 cells, AR signal was detected in the cytoplasm before adding DHT (Fig. 8A and C). After the treatment with DHT, AR formed fine foci in the nucleus (Fig. 8D and F). On the other hand, a markedly reduced number of nuclear foci (Fig. 8G and I) or even no foci (Fig. 8J and L) were observed in the DHT-treated MC3T3-E1 cells when both AR-GFP and YFP-Tob1 were cotransfected. No significant change was observed in the intracellular distribution of YFP-Tob1 before and after the addition of DHT. The inhibition of the AR foci formation by Tob1 was well consistent with the suppression of the AR-mediated transactivation function by Tob1 assessed by the luciferase reporter assay.

Fig. 2. Tob proteins suppress AR- and ERα-mediated transcriptional activation in osteoblastic cells. (A) Immunoblot analysis of human Tob family-YFP fusion proteins. Cell lysates were collected from MC3T3-E1 cells transfected with the expression vectors for Tob family proteins fused with YFP and were subjected to SDS-polyacrylamide gel electrophoresis (lanes 1 and 2, YFP-Tob1; lane 3, YFP-Tob2; lane 4, YFP-PC3). After proteins were transferred onto the nitrocellulose membrane, anti-Tob1 (lane 1) or anti-GFP (lanes 2–4) antibody was reacted with each membrane for detection of the fusion proteins. Asterisks (*) indicate the YFP fusion protein of each Tob family protein. Positions of protein size markers are shown on the left. (B) Suppression of AR-mediated transcriptional activation by Tob proteins. MC3T3-E1 osteoblastic cells were transfected with 0.1 μg of the AR expression vector, 0.1 or 0.3 μg of the Tob1, Tob2, PC3 expression vector, or the empty vector (Vec), 0.5 μg of pGL3-MMTV and 3 ng of pRL-CMV. The cells were cultured in the absence (−) or presence (+) of 10^{-8} M DHT for 24 h and the luciferase activities were measured. Left three bars show the results of cells without being transfected with the AR expression vector. Bars show the fold change in the luciferase activity relative to the value by the wild type AR without DHT. The average of three independent experiments is shown with the standard deviation. $^{*}P < 0.05$. (C) Suppression of ERα-mediated transcriptional activation by the Tob protein. MC3T3-E1 cells were cotransfected with 0.1 μg of pSG5-ERα, 0.1 or 0.3 μg of the pYFP-Tob1, pYFP-Tob2 or the empty vector (Vec), 0.5 μg of pERE2-tk109-luc as a reporter plasmid and 3 ng of pRL-CMV as an internal control. Three hours after transfection, 10^{-6} M estradiol (E_2) was added. Luciferase activity was measured after 24 h incubation. Relative luciferase activity is shown. Bars show the fold change in the luciferase activity relative to the value without the ligand. The mean values and the standard deviation from three independent experiments are shown. $^{*}P < 0.05$.

4. Discussion

In the present study, we demonstrated that expression of Tob protein in MC3T3-C1 osteoblastic cells suppressed the ligand-dependent transactivation function of steroid hormone

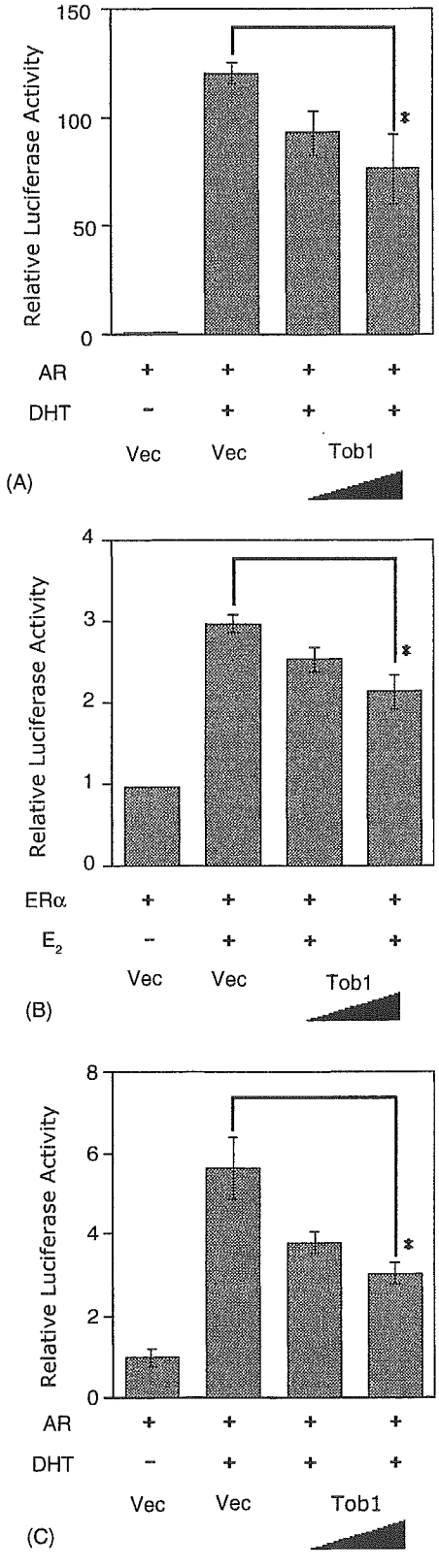

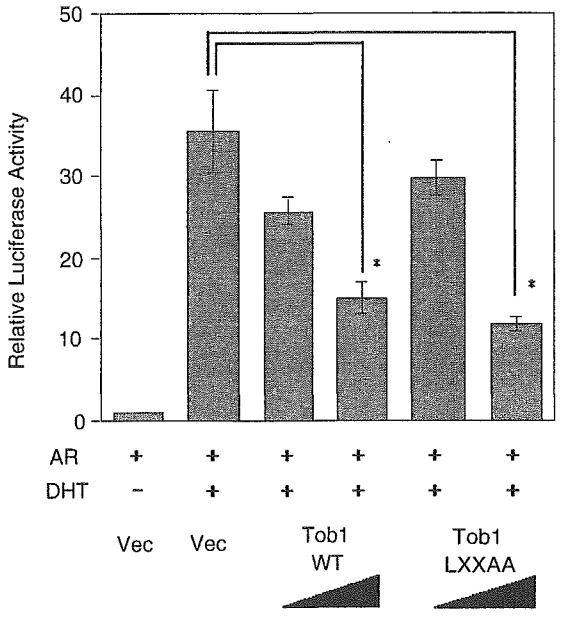

Fig. 4. Suppression of AR-mediated transcriptional activation by a Tob1 LXXAA mutant. The wild type (WT) and mutated (LXXAA) Tob1, carrying amino acid substitutions in its LXXLL motif (LXXLL to LXXAA), were expressed in MC3T3-E1 cells with the AR expression vector and reporter plasmids. The luciferase assay was performed as described in Section 2. The average of three independent experiments is shown with the standard deviation. $^{*}P < 0.05$.

receptors, AR and ERα, and inhibited the ligand-dependent nuclear foci formation of AR.

Some of the Tob family proteins have an LXXLL motif that has been identified in many nuclear receptor coregulators. Through this motif, these coregulators can directly interact with nuclear receptors to modulate the transcriptional activation (Leo and Chen, 2000; Aranda and Pascual, 2001; Cheng et al., 2002; Heinlein and Chang, 2002). It has been reported that two Tob family proteins, BTG1 and BTG2, can either enhance or repress ligand-induced transactivation function of ERα, depending on the promoter context. BTG proteins do not directly interact with ERα, but BTG1 can

Fig. 3. Tob protein-induced suppression of AR- or ERα-mediated transactivation of MMTV (A), ERE2-tk109 (B) and PSA (C) promoter in PC3 (A and B) and COS-7 (C) cells. (A) Prostatic carcinoma cells, PC3, were cotransfected with AR expression vector (0.1 μg/well), 0.5 μg of pGL3-MMTV, 3 ng of pRL-CMV and 0.2 or 0.5 μg of the pYFP-Tob1 or the empty vector (Vec). Three hours after transfection, the ligand was added. Luciferase activity was measured after 24 h incubation. (B) PC3 cells were cotransfected with 0.1 μg/well of pSG5-ERα, 0.5 μg/well pERE2-tk109-luc, 3 ng of pRL-CMV and 0.2 or 0.5 μg of the pYFP-Tob1 or the empty vector (Vec). After the transfection, cells were treated with or without 10^{-6} M E_2 for 24 h and then luciferase assay was performed. (C) COS-7 cells were cotransfected with pCMV-hAR (0.1 μg/well), 0.3 μg of pGL3-PSA, 3 ng of pRL-CMV and 0.2 or 0.5 μg of the pYFP-Tob1 or the empty vector. After the transfection, cells were incubated in the absence or presence of 10^{-8} M DHT for 24 h and then luciferase assay was performed. Relative luciferase activity is shown and bars represent the fold change in the luciferase activity relative to the value without the ligand. The mean values and the standard deviation from three independent experiments are shown. $^{*}P < 0.05$.